RESEARCH REPORT

VTT-R-09382-11

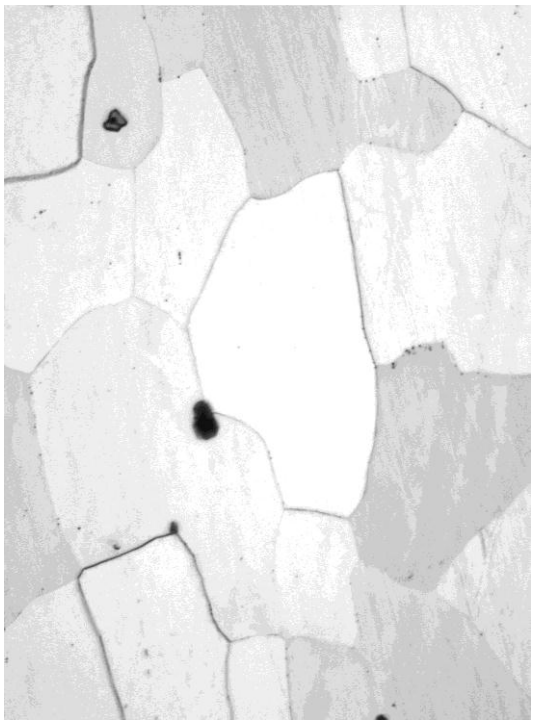

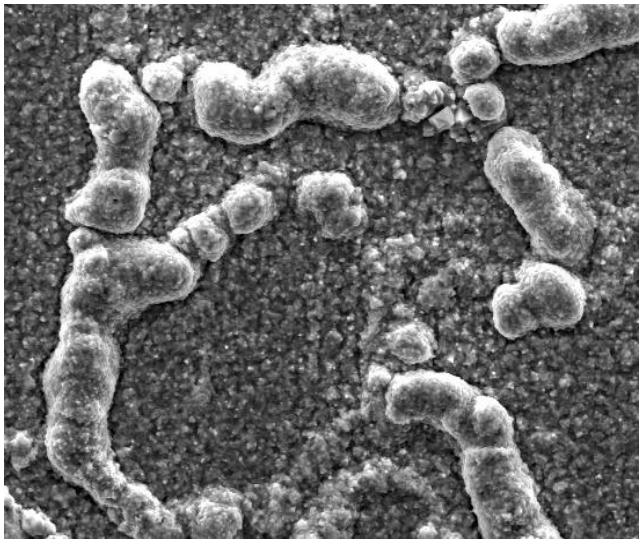

Oxidation and degradation of ferritic alloys for SOFC interconnectors

Authors: Juha Veivo, Sanni Yli-Olli, Pertti Auerkari, Stefan Holmström, Petra Jauhiainen

Confidentiality: Public

Report's title	
Oxidation and degradation of ferritic alloys for SOFC interconnectors	
Customer, contact person, address FINNSTACK / SOFCPOWER	Order reference
Project name SOFCPOWER	Project number/Short name 26068
Author(s) Juha Veivo, Sanni Yli-Olli, Pertti Auerkari, Stefan Holmström, Petra Jauhiainen	Pages 42/-
Keywords SOFC, interconnector, degradation	Report identification code VTT-R-09382-11

Summary

Oxidation and degradation of the ferritic stainless steels has been studied as candidate SOFC interconnector alloys. In terms of internal degradation, exposure at 740°C up to 5000 h mainly resulted in gb carbide coarsening in alloy 430, and mainly in grain growth in alloys ZMG 232 and Crofer 22 APU. Alloy 430 showed slowest and ZMG 232 highest oxidation rate in dry air, with mass change reasonably consistent with parabolic oxidation at least up to 500 h. By 5000 h of exposure Crofer 22 APU and alloy 430 (but not ZMG 232) showed signs of oxide spallation. The oxides that did not spall were about 3-4 µm in thickness after 5000 h at 740°C. The oxidation rate constants from this work appear higher than those from the literature, but in a similar isothermal range and in the same materials order. Up to 5000 h the chemical composition of the surface oxide showed mostly similar change for all tested alloys, with decreasing Fe content and increasing Mn content. The Cr content of the surface oxide increased from 18-22% to 35-41% in 500 h and was thereafter constant or slightly decreasing to about 24-40% after 5000 h. No significant difference was observed in the surface composition of any of the three alloys when comparing the regions within and outside the contact to a cell cathode surface. The oxide surface of alloy 430 was relatively uniform, and no distinct precipitates were seen below the oxide. The oxide surfaces on ZMG 232 and Crofer 22 APU showed Cr- and Mn-rich oxides precipitating at the oxide grain boundaries to form a network that was further coarsening during annealing. All alloys showed a Cr-rich layer on top and a Si-rich discontinuous layer next to the metal. Below the surface oxides the alloys ZMG 232 and Crofer 22 APU showed a layer with relatively large Al- and Ti-rich precipitates. For all tested alloys in contact with the cell cathode, the Cr content of the cell surface started to increase by 500 to 5000 h of exposure. Therefore, Cr evaporation is likely to be an issue for all alloys in long term service at comparable or even lower temperature levels. Protective solutions to avoid cathode poisoning appear necessary even for steels like ZMG 232 and Crofer 22 APU that have been designed for SOFC interconnector service.

Confidentiality	Public

Espoo 28.12.2011

Written by	Reviewed by	Accepted by
Juha Veivo Research Scientist	Jorma Salonen Principal Scientist	Pentti Kauppinen Technology manager

VTT's contact address
POB 1000, FI-02044 VTT, Finland, tel +358 20 722 111; juha.veivo@vtt.fi

Distribution
VTT Archive 1 copy

Preface

This work was initiated in the VTT research theme Clean World and completed as a part of the SOFCPOWER project. The authors wish to thank Dr. Karri Osara of Outokumpu Research for help in materials access and analytics during the course of this work.

Otaniemi, 28.12.2011

Authors

Contents

1 Introduction

1.1 SOFC interconnector materials - general

The metallic interconnectors of solid oxide fuel cells (SOFC) need to provide sufficient charge transport during cell operation at high temperature. Three SOFC interconnector alloys are considered here from the point of view of oxide growth and thermal degradation, particularly for the cathode side of intermediate temperature SOFC´s. The selected materials are ferritic stainless alloys, including one common standard grade (alloy 430) and two alloys (Crofer 22 APU and ZMG 232) specifically designed for interconnector service.

1.2 Objectives

This work aims to explore the characteristic features of oxidation and thermal degradation in the selected ferritic stainless steels at the service temperatures of SOFC interconnectors.

2 Materials and methods

2.1 Materials

The nominal composition of the selected interconnector alloys are shown in Table 1. All alloys are ferritic stainless steels, one standard grade (alloy 430) and two dedicated commercial alloys (Crofer 22 APU, ZMG 232) specifically designed for interconnector service. All materials were obtained from the suppliers as 2.5-3.0 mm plates.

Table 1. Test alloys and their nominal compositions

Alloy	Supplier	Nominal composition (wt-%)
430	Outokumpu	Cr 16-18, C max 0.12, Mn max. 1.0, Si max. 1.0, Fe bal.
Crofer 22 APU	ThyssenKruppVDM	Cr 22, C 0.013, Mn 0.8, Si 0.5, Ti 0.2, La 0.2, Fe bal.
ZMG 232	Hitachi Metals	Cr 22, C 0.02, Mn 0.5, Ni 0.26, Al 0.21, Zr 0.22, La 0.04, Fe bal.

2.2 Methods

Test coupons with a size of 15x15mm were machined from the supplied plates. All sides of test coupons were ground to grit 1200 and washed first in acetone, rinsed in distilled water and rewashed in ethanol prior to drying and testing. Each coupon was also measured for dimensions (with a Mitutoyo caliper, uncertainty ± 0.005 mm) and mass (with a Mettler balance AT261, uncertainty ± 0.003 mg) before testing. The test coupons and the test arrangement are shown in Fig. 1 and Fig. 2.

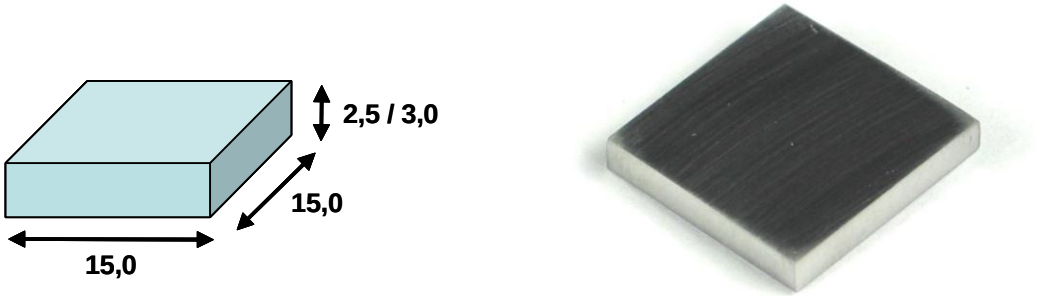

a) *b)*

Fig. 1. Test coupon: a) nominal dimensions; b) coupon before testing.

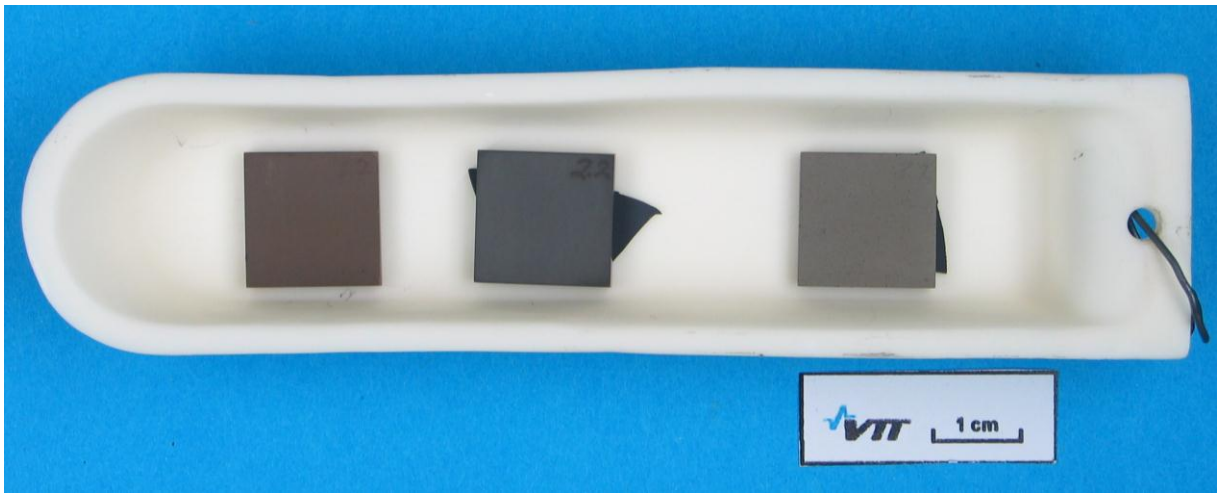

Fig. 2. Test arrangement with test coupons placed on pieces of planar SOFC cells.

The test coupons were subjected to annealing in dry laboratory air (about 50% relative humidity at room temperature) at 740°C for test periods varying from 5 hours to 5000 hours. In all cases the test coupons were placed on the cathode side of a planar piece of a SOFC cell (InDec).

After annealing sequence, the test coupons were weighed again and subjected to metallographic and surface analysis by optical and scanning electron microscopy (OM, SEM), and EDS. Metallographic and chemical analyses were also performed on the surfaces of the cells that were in contact with the test coupons.

The results were analysed particularly with respect to signs of thermal degradation, changes in the surface structures and/or chemical composition near the surfaces.

3 Results

3.1 Mass change of the test coupons

The measured mass change of the test coupons is shown in Fig. 3 for all test alloys up to 5000 hours of annealing at 740°C. A somewhat more pronounced oxidation appears to occur in the

alloys ZMG 232 and Crofer 22 APU than in the alloy 430. All alloys appear to reach a mass change of about 0.1-0.2 mg/cm^2 in air within 1000 h. The oxide on Crofer 22 APU has spalled off between 500 and 5000 h of testing. Except for apparent initial deviation in Crofer 22 APU, all materials seem to have obeyed a roughly linear time dependence on the logarithmic scale as seen in Fig. 3.

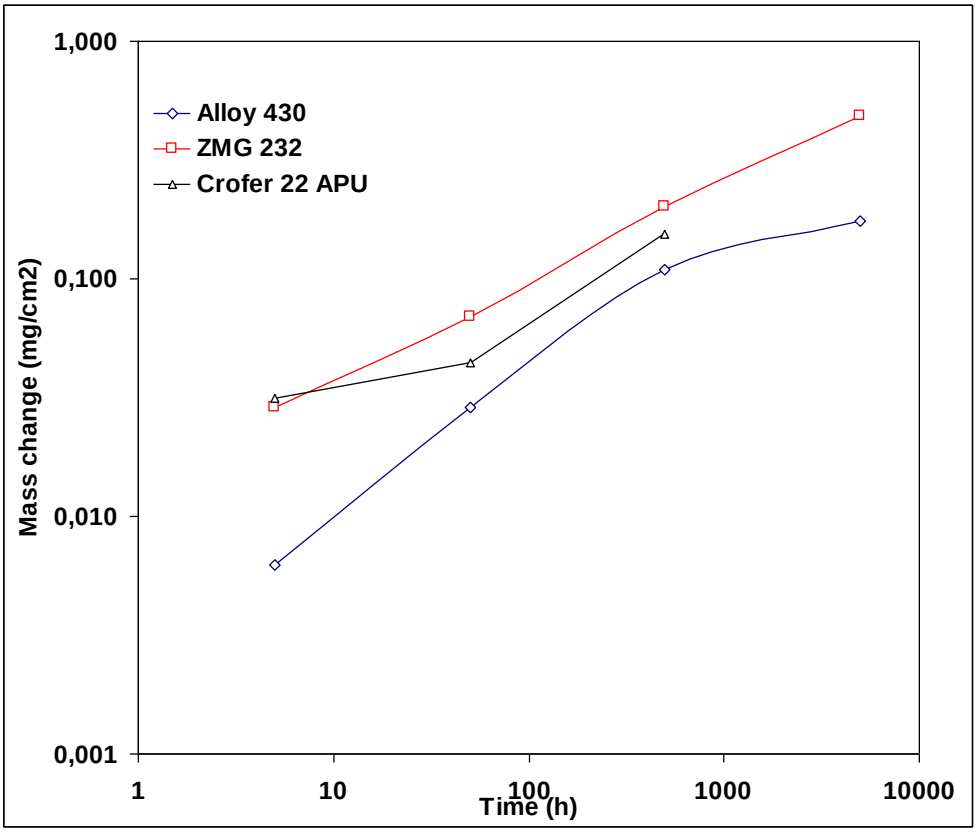

Fig. 3. Mass change in test materials up to 5000 hours of annealing at 740°C. The oxide on Crofer 22 APU has spalled off between 500 and 5000 h of testing.

The mass change Δm of Fig. 3 can be expressed by fitting to the data the power law oxidation expression for expired time t as follows:

$$\log \Delta m = 0.0024 \cdot t^{0.6217} \text{ for alloy 430} \quad (1)$$

$$\log \Delta m = 0.0145 \cdot t^{0.4133} \text{ for ZMG 232} \quad (2)$$

$$\log \Delta m = 0.0054 \cdot t^{0.5394} \text{ for Crofer 22 APU} \quad (3)$$

The expressions for alloy 430 and Crofer 22 APU only apply to 500 h due to oxide spallation after this time. In the above expressions (1-3) Δm is given in mg/cm^2 and time *t* in hours.

3.2 Degradation of alloy 430

3.2.1 Contact surfaces of alloy 430

The observed changes in the chemical composition of the oxidised surface of alloy 430 in contact with the cell cathode are shown in Fig. 4. Increase in manganese content, slight

decrease in Cr and clear decrease in iron content is evident on these surfaces. By about 5000 h of exposure, the Cr and Mn contents are approaching 30-35% while Fe content is small (2%). No significant difference was observed when comparing the chemical compositions between the regions within and outside the contact to the cell.

The appearance of the oxide surface after 500 h and 5000 h within and outside cell contact is shown in Fig. 5 to Fig. 8. Up to 500 h the oxide surfaces appear fairly even and without other features than apparent surface particles size of up to 3 µm. The cross sections of the oxide surface after 500 h and 5000 h of exposure with and without cathode contact are shown in Fig. 9 to Fig. 12. The oxides appear to grow to approximately thickness of 4µm without cathode contact and to about 3 µm with cathode contact in 5000 h. The element maps of the oxide surface cross section after 5000 h in contact with cathode are shown in Fig. 13 and Fig. 14. The appearance of the contact area of the cell is shown in Fig. 15 to Fig. 18. After 50 to 500 h of annealing, elevated chromium content was observed in EDS analysis of the contact area of the cell cathode. Particularly high chromium content of about 25% was observed on the dark areas of the cell surface after 5000 h of exposure (Fig. 19).

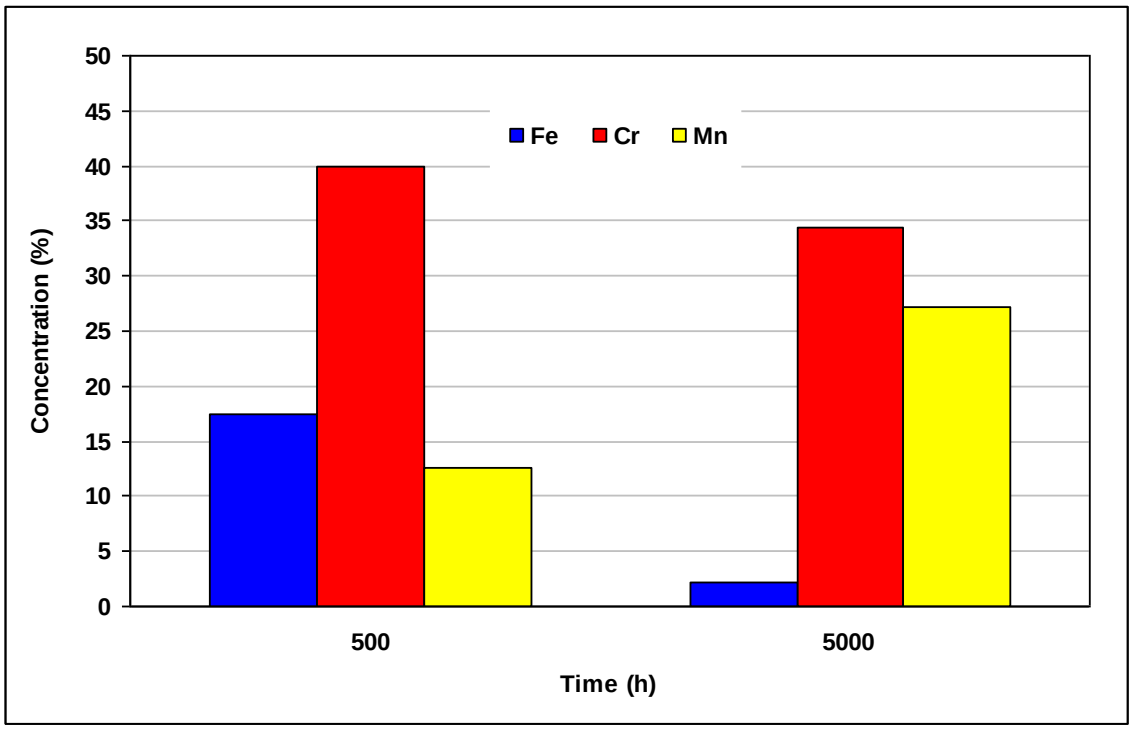

Fig. 4. Observed change in concentration of selected elements on the surface of alloy 430 at 740°C in contact with the cathode side of a SOFC cell (EDS analysis of oxide surface).

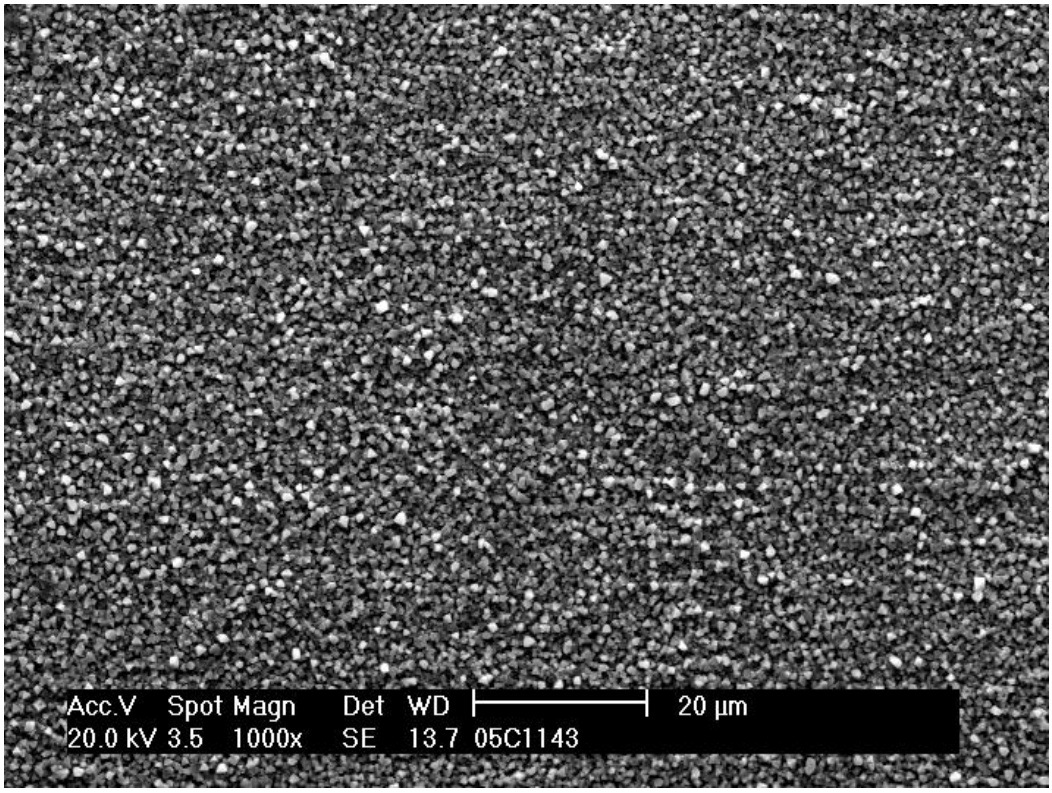

Fig. 5. Surface appearance of alloy 430 after 500 h at 740°C in contact with SOFC cell cathode.

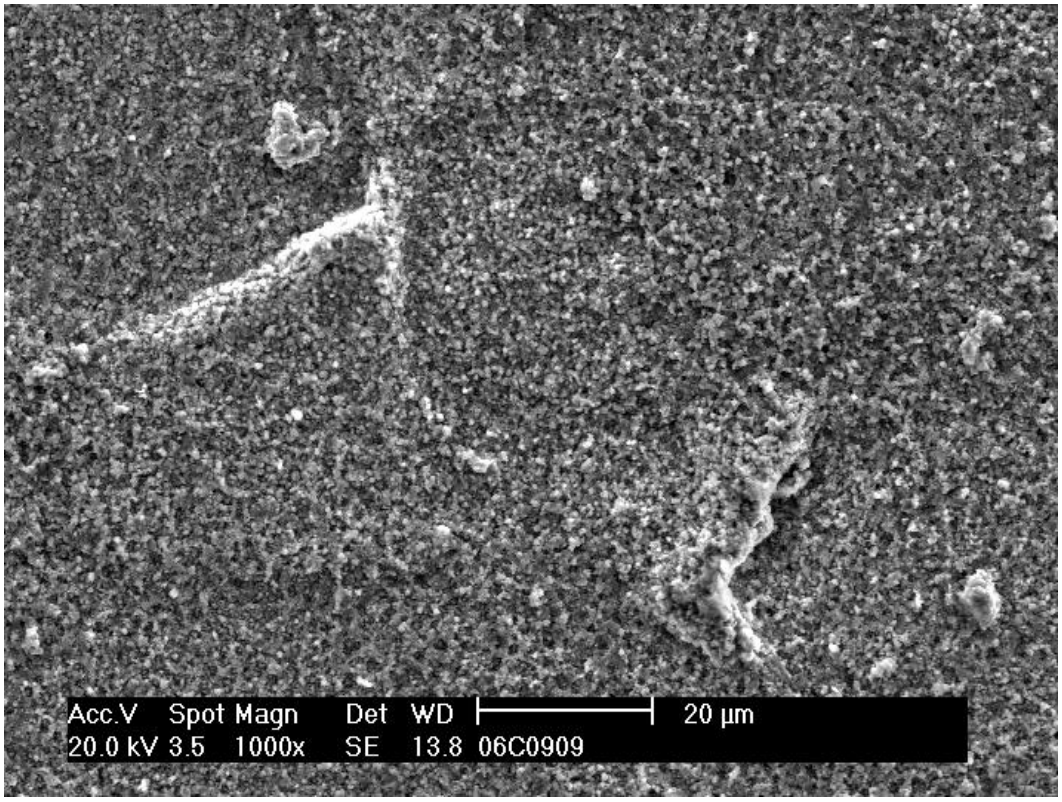

Fig. 6. Surface appearance of alloy 430 after 5000 h at 740°C in contact with SOFC cell cathode.

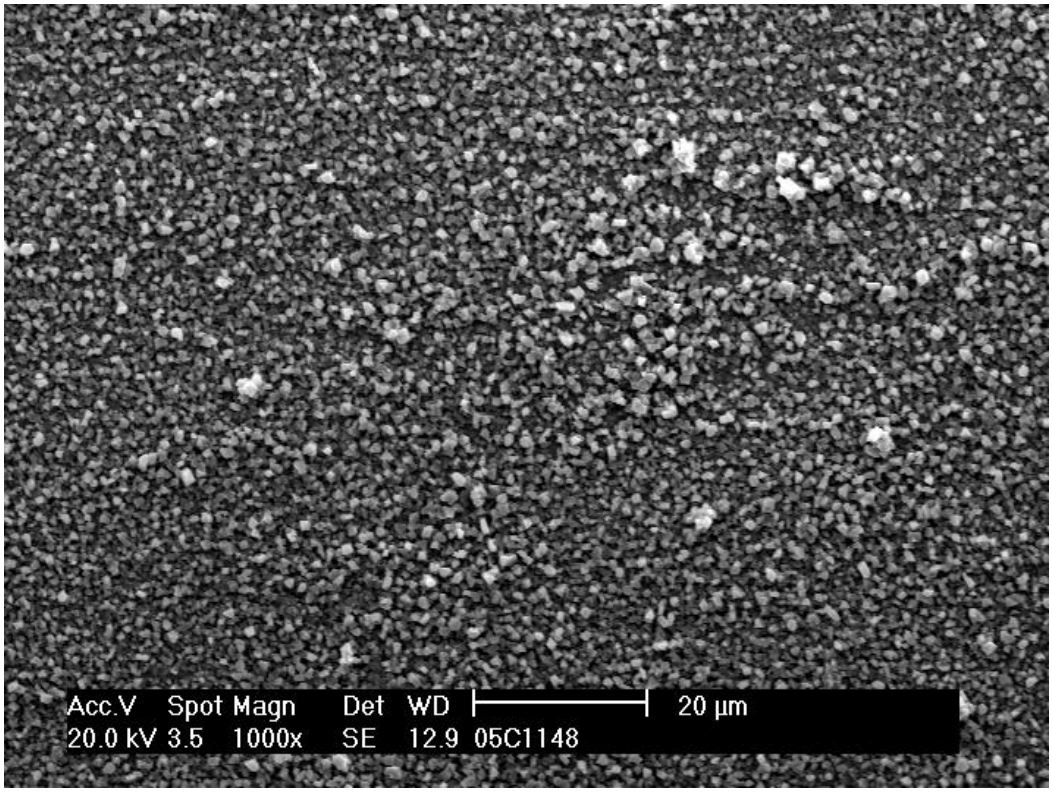

Fig. 7. Surface appearance of alloy 430 after 500 h at 740°C outside cell contact.

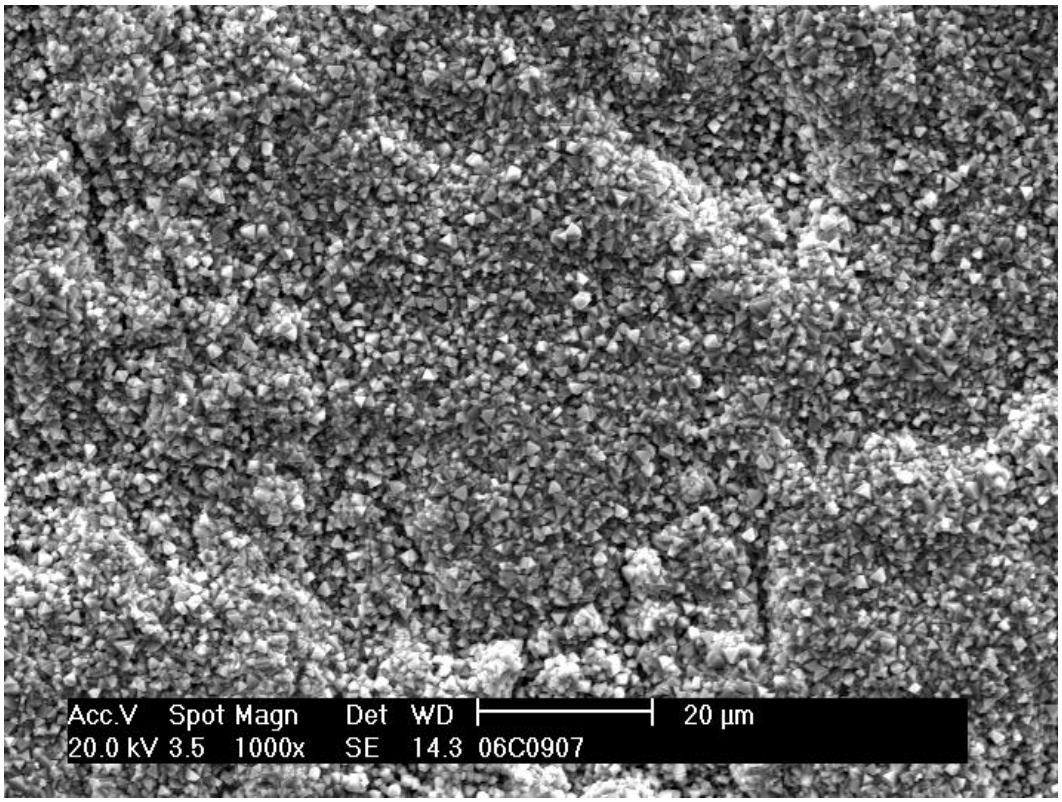

Fig. 8. Surface appearance of alloy 430 after 5000 h at 740°C outside cell contact.

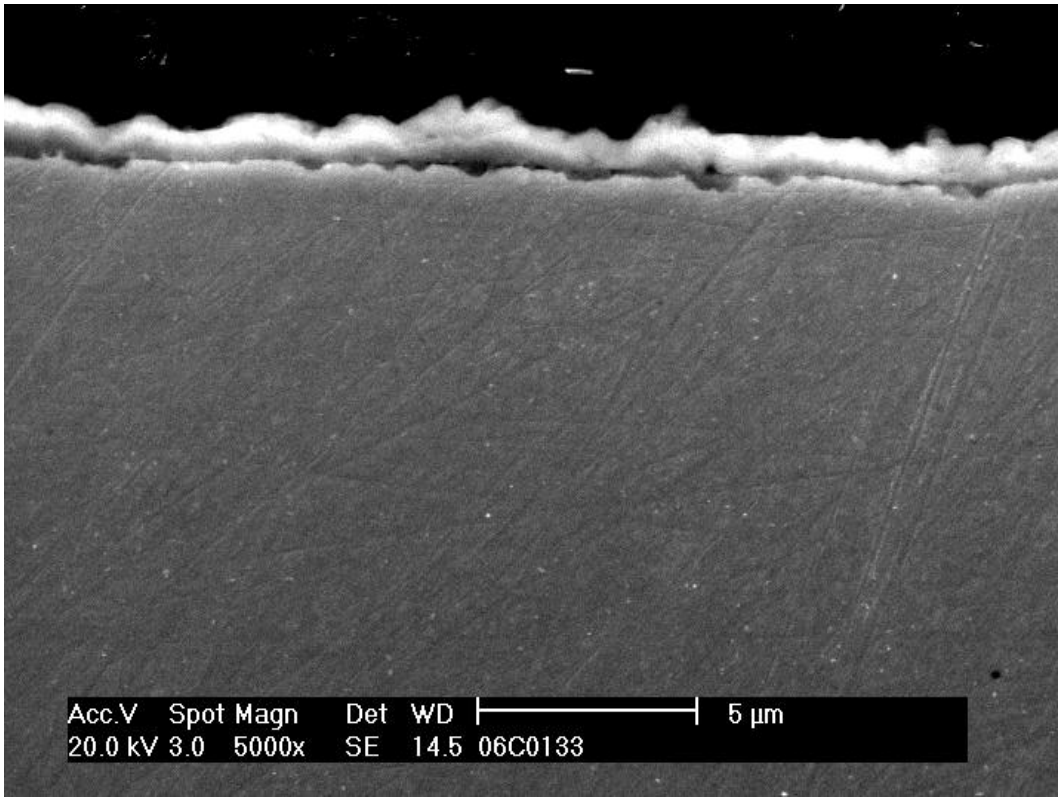

Fig. 9. Cross-section of alloy 430 after 500 h at 740°C in cathode contact.

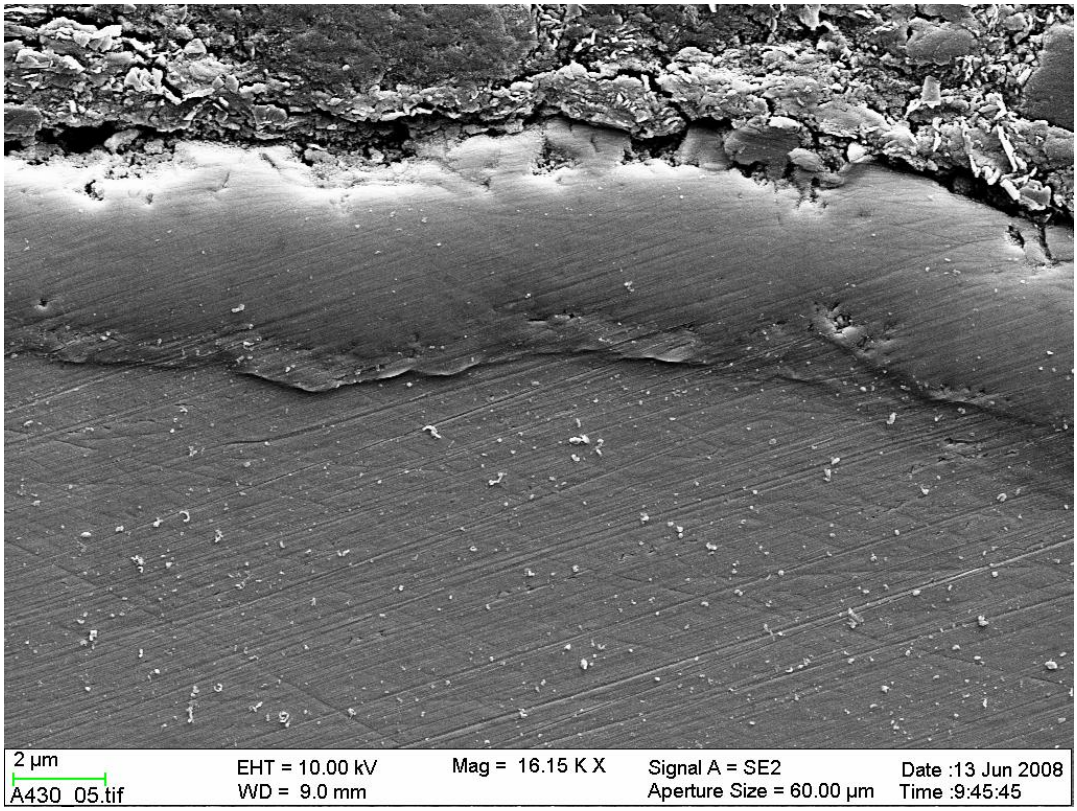

Fig. 10. Cross-section of alloy 430 after 5000 h at 740°C in cathode contact.

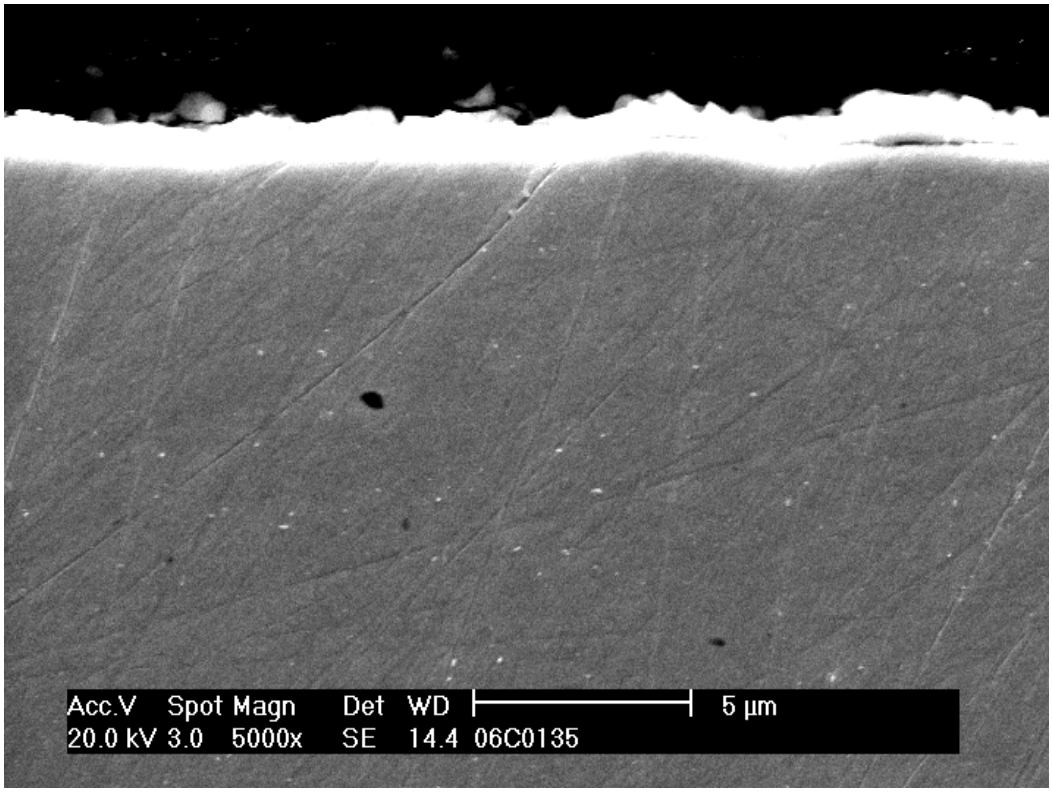

Fig. 11. Cross-section of alloy 430, after 500 h at 740°C outside cathode contact.

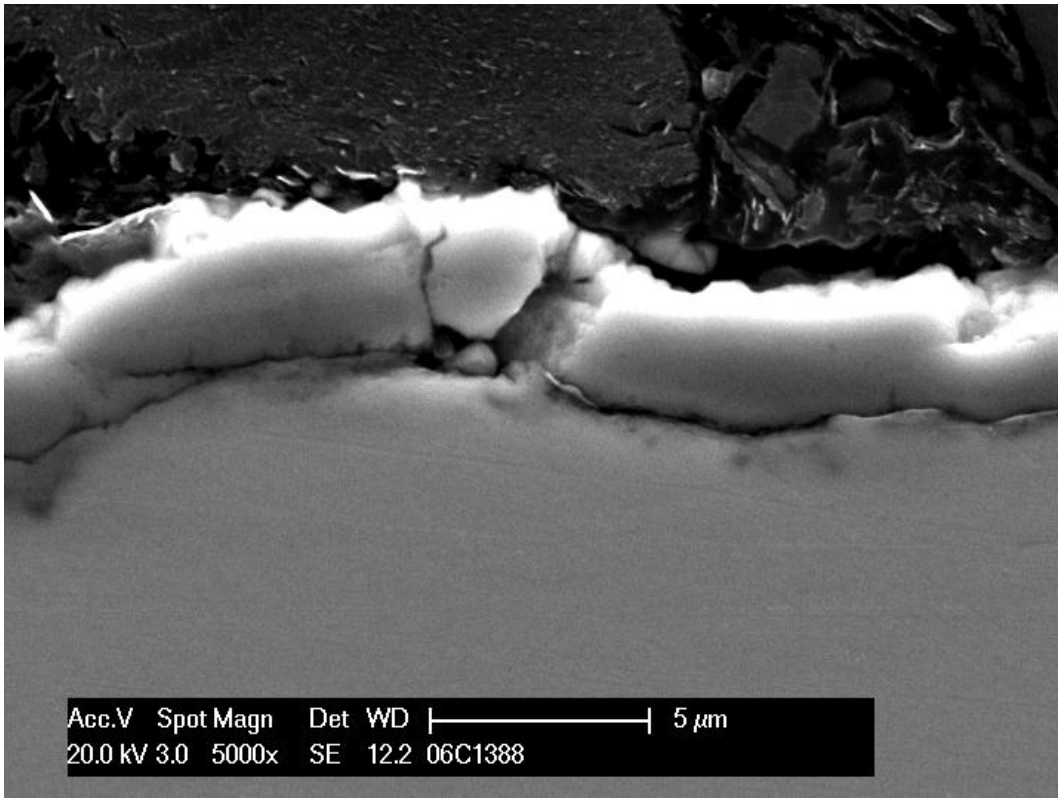

Fig. 12. Cross-section of alloy 430, after 5000 h at 740°C outside cathode contact.

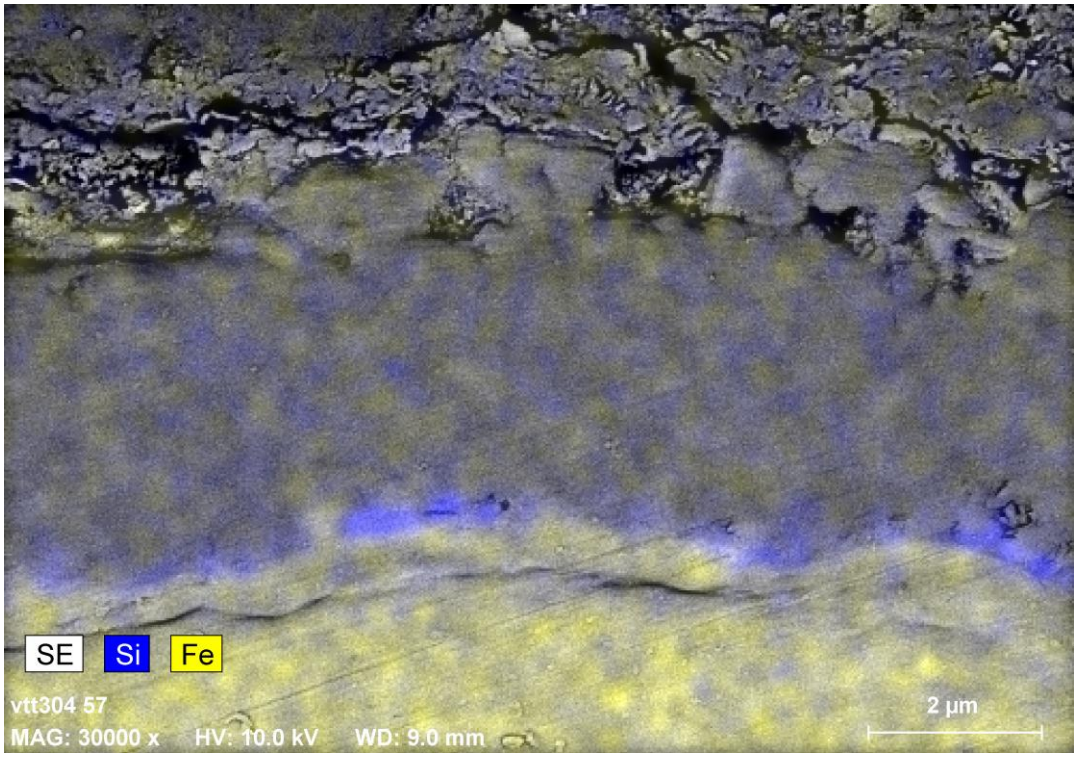

Fig. 13. Element map of Si and Fe for alloy 430 surface cross section of the cathode side after 5000 h at 740°C

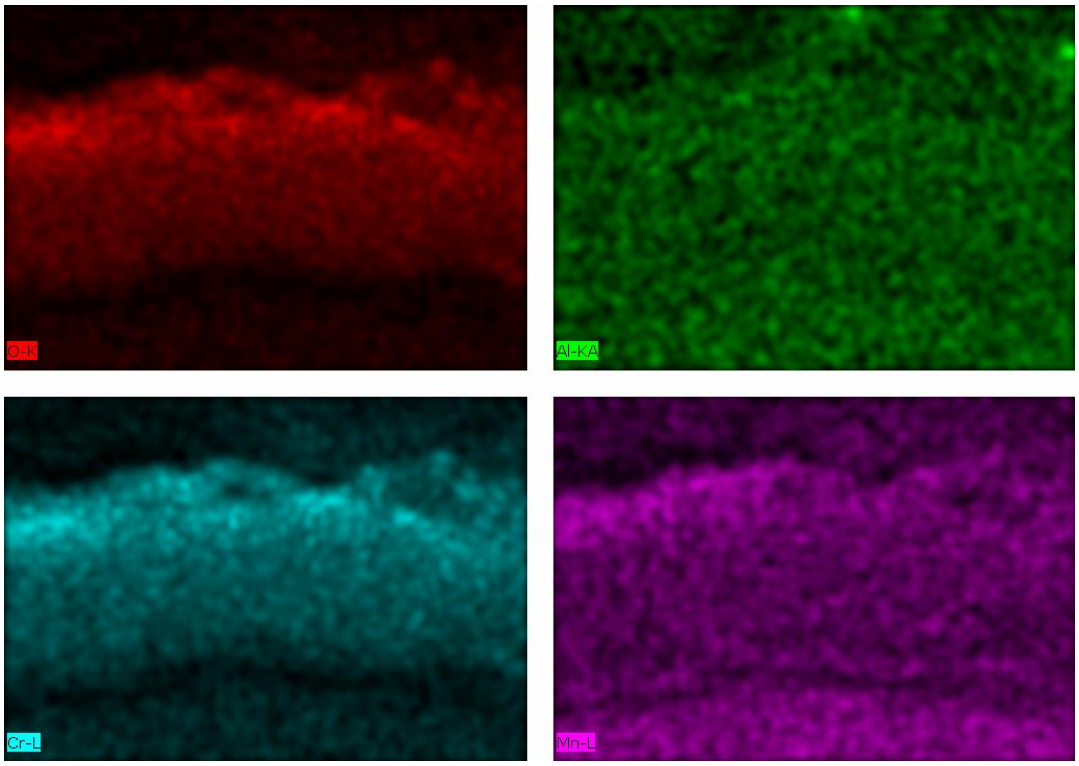

Fig. 14. Element maps of O, Al, Cr and Mn for alloy 430 surface cross section of the cathode side after 5000 h at 740°C (same location as in Fig 13)

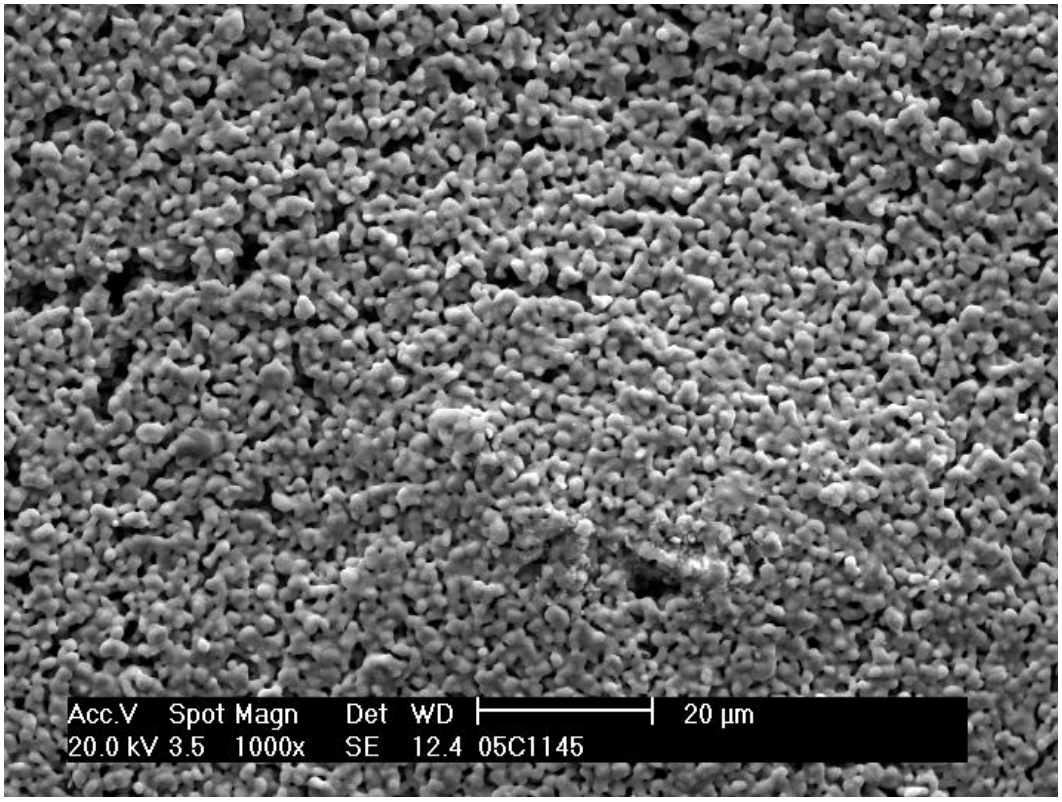

Fig. 15. The appearance of the cathode side cell surface after 500 h at 740°C in contact with alloy 430. Note a lighter area with a diameter of about 50 µm.

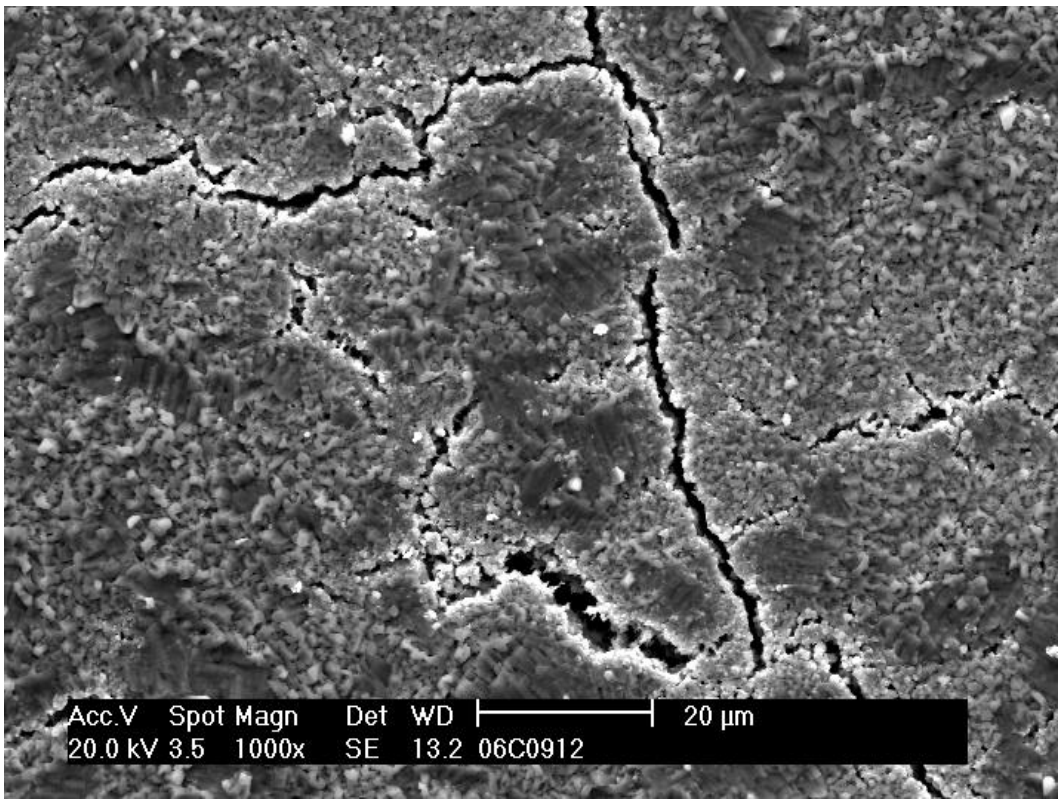

Fig. 16. The appearance of the cathode side cell surface after 5000 h at 740°C in contact with alloy 430. Note that the cracks could have been caused at sampling of the cell pieces.

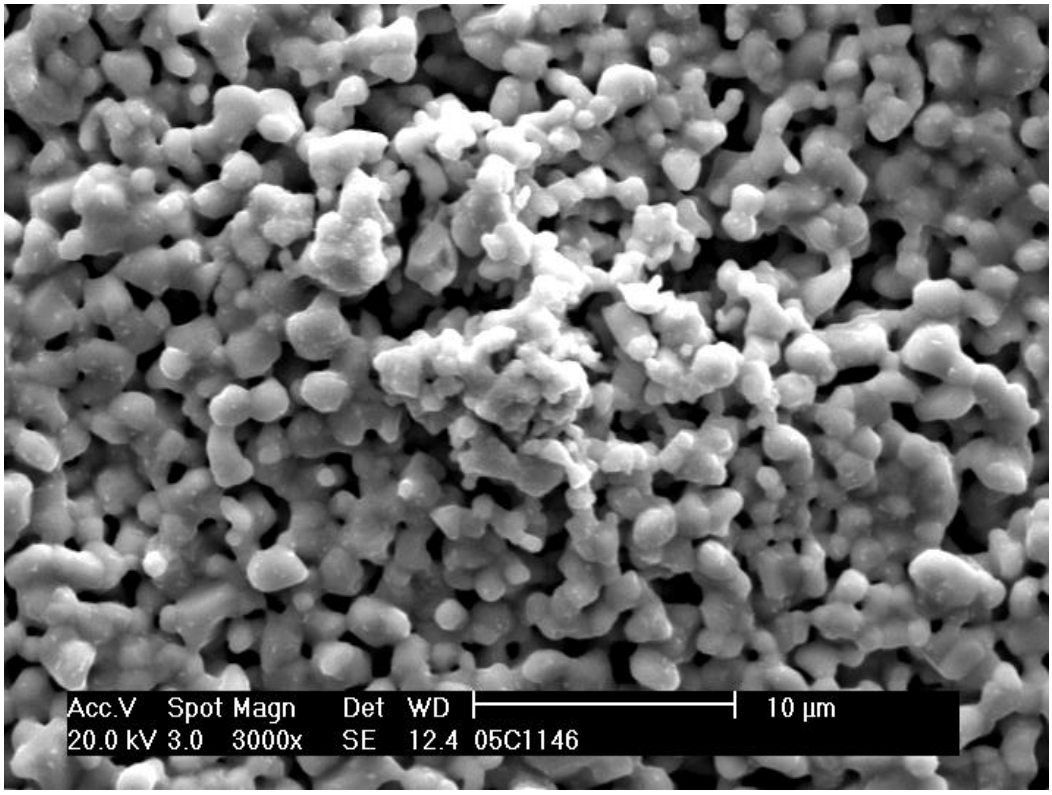

Fig. 17. Partial magnification of the lighter region of Fig. 15, suggesting possible contact and contamination from the bipolar plate alloy (500 h).

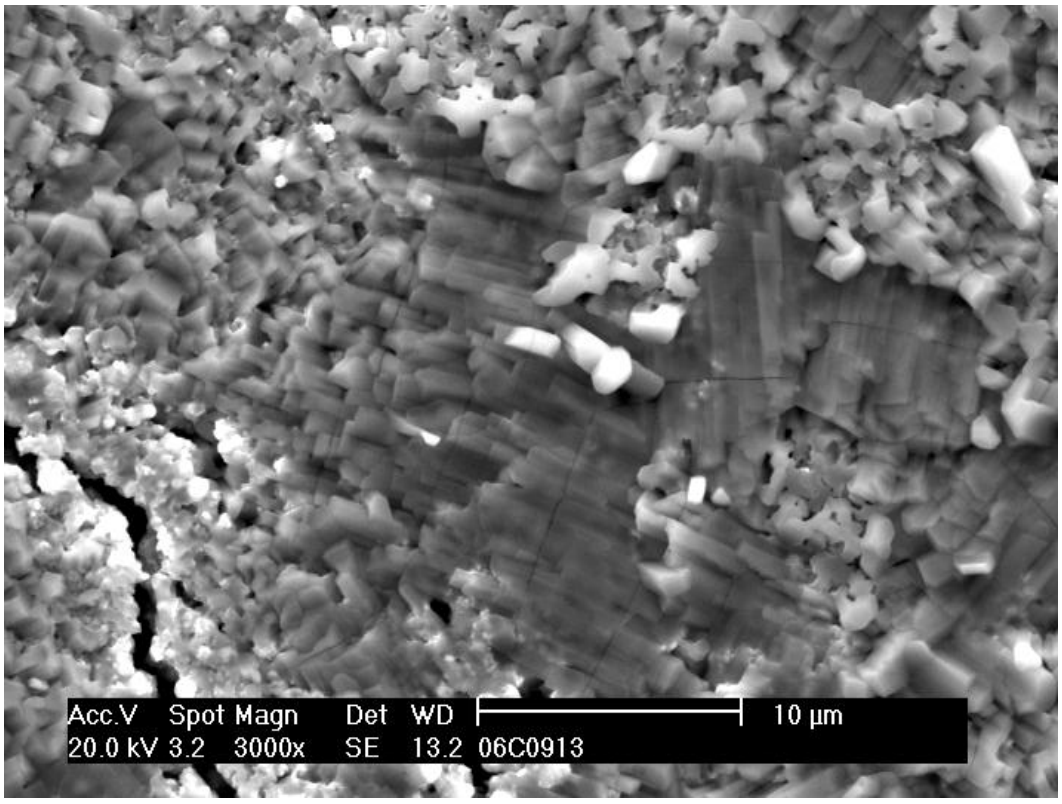

Fig. 18. Partial magnification of the lighter region of Fig. 16, suggesting possible contact and contamination from the bipolar plate alloy (5000 h).

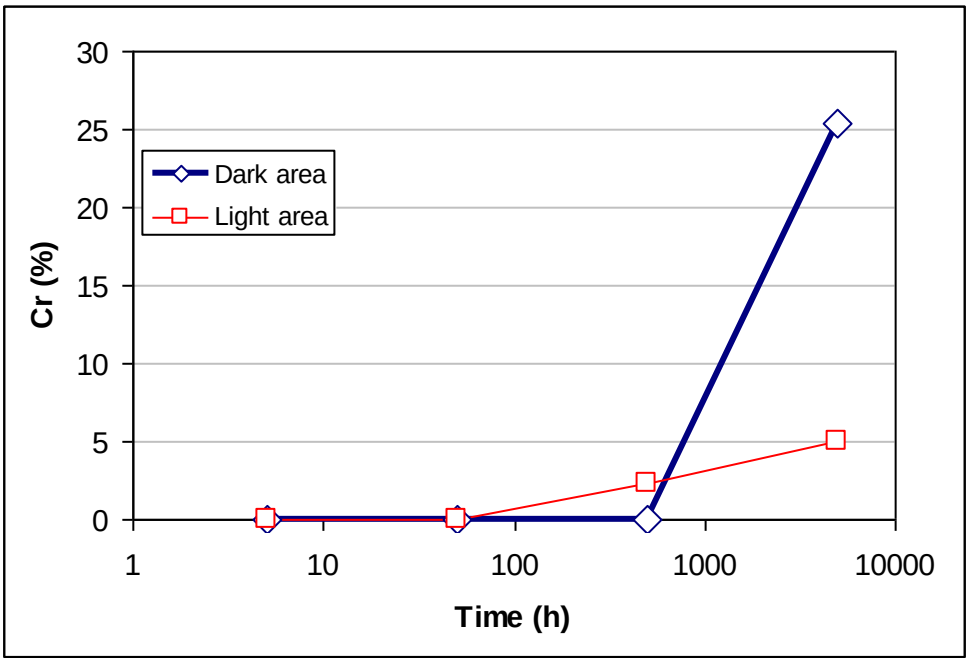

Fig. 19. The chromium content on the contact surface of the SOFC cell (with alloy 430, EDS analysis).The light areas on the cathode surface are slightly elevated regions and the dark areas lower plateaus (Fig. 15 to Fig. 18).

3.2.2 Microstructural evolution of alloy 430

Annealing at 740°C can also have an impact on the microstructures of the metal below the oxide. Such microstructures are shown in Fig. 20 to Fig. 22 for the initial state and after 500 and 5000 h of exposure. It can be seen that at this level of detail, the main change of the microstructure is limited to carbide precipitation and coarsening at the grain boundaries. A peculiar feature already in the initial state (Fig. 20) appears as abundant carbide strings in the microstructure.

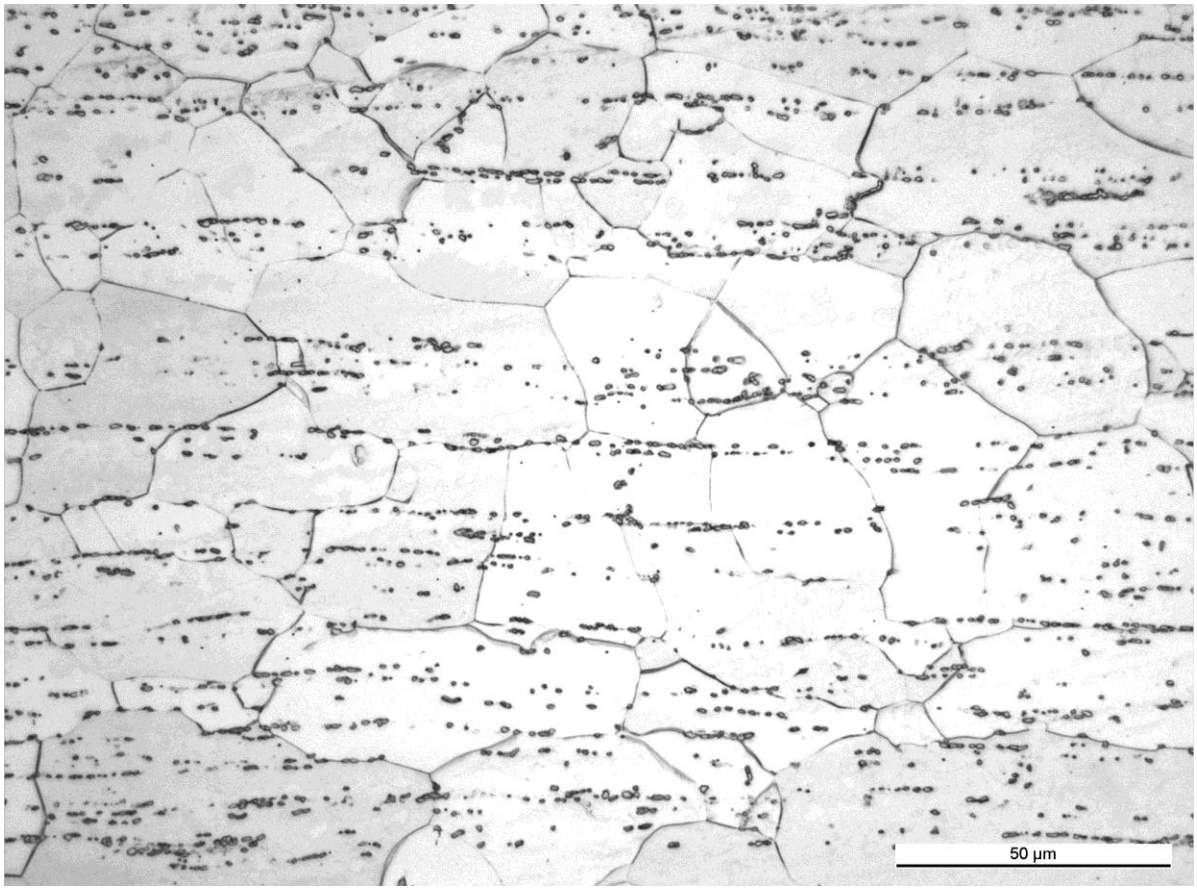

Fig. 20. The microstructure of alloy 430 as received.

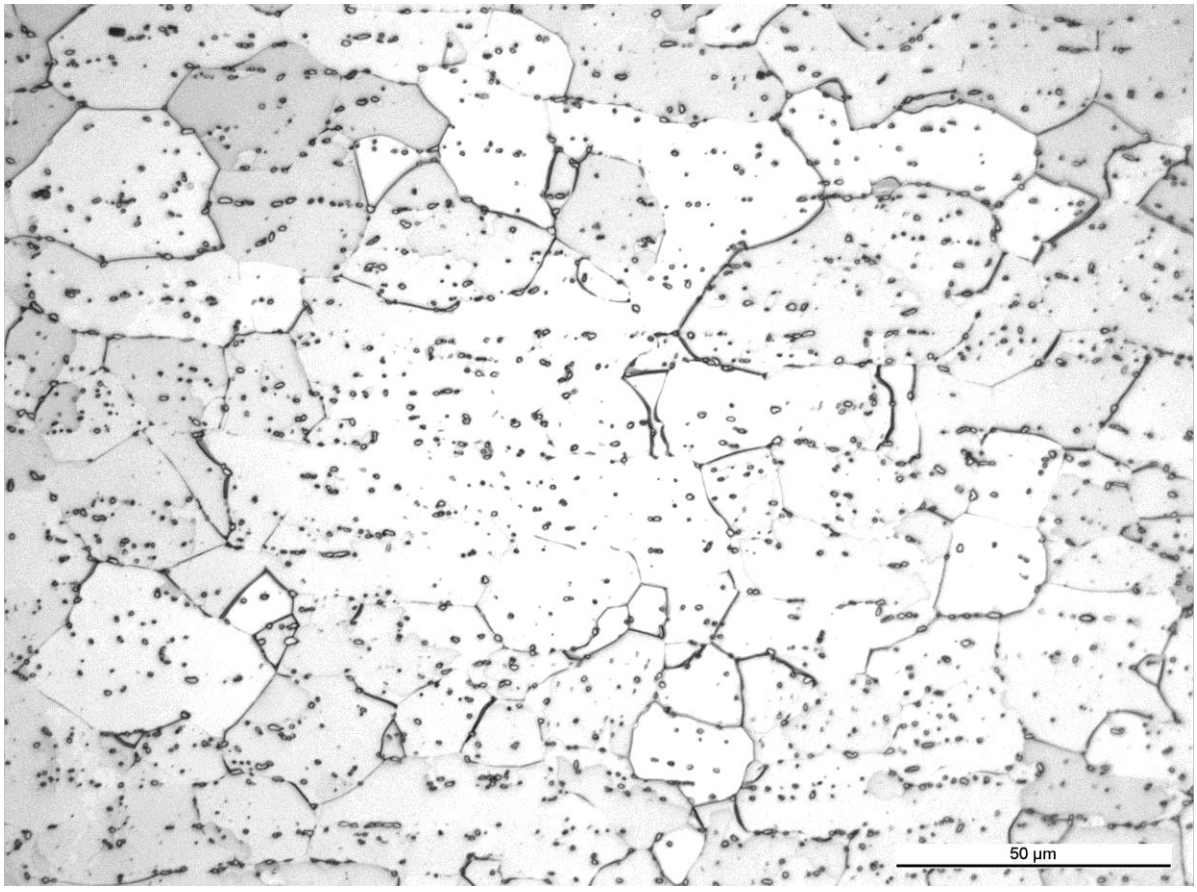

Fig. 21. The microstructure of alloy 430 after 500 h of exposure.

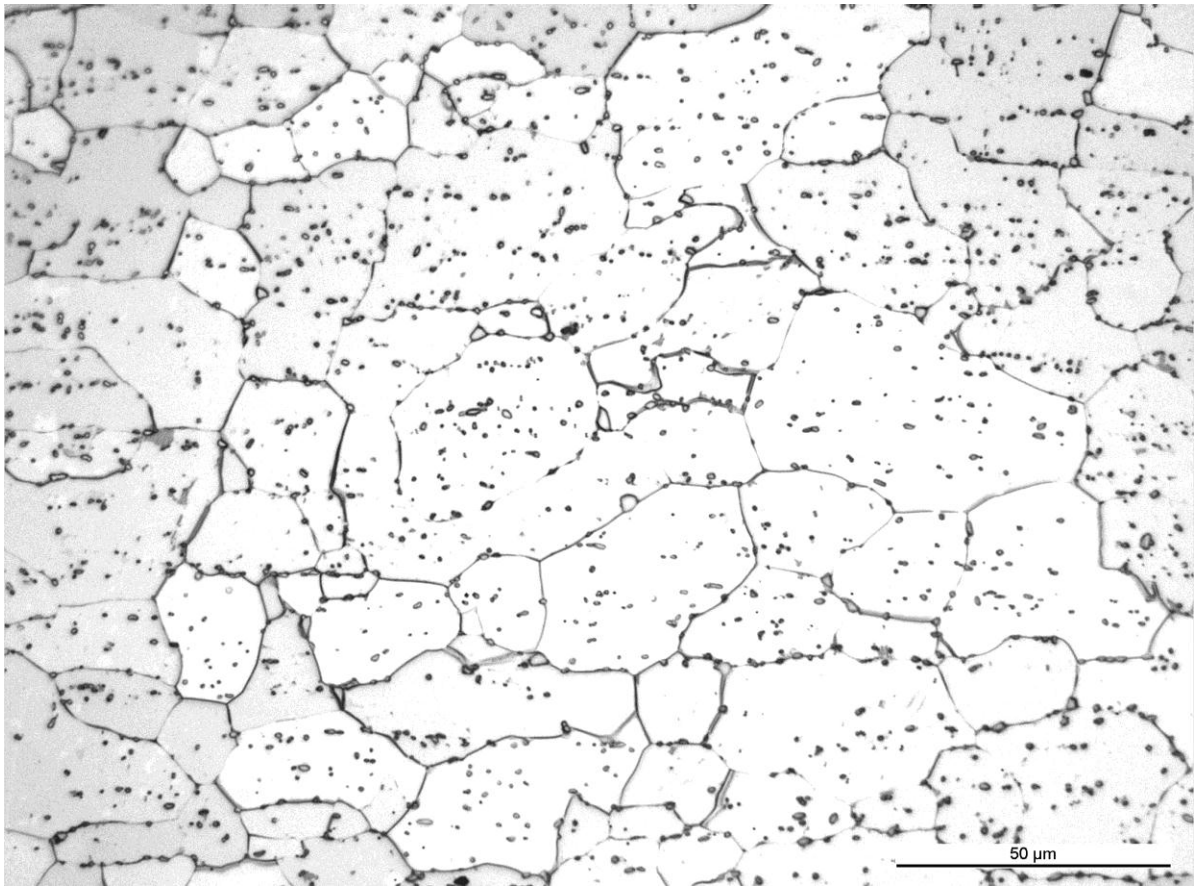

Fig. 22. The microstructure of alloy 450 after 5000 h of exposure.

3.3 Degradation of ZMG 232

3.3.1 Contact surfaces of ZMG 232

The surface composition of ZMG 232 is shown in Fig. 23 after test periods in contact with the cell cathode. Again, increasing manganese content and decreasing iron and chromium contents are seen on the oxidised metal surfaces. After 5000 h the surface Cr and Mn content has reached about 25-30% and iron content has decreased to about 13%. No significant difference was observed when comparing the chemical compositions of the metal surface oxides between the regions within and outside the contact to the cell. The appearance of the metal surfaces within and outside the contact area to the cell after 500 h and 5000 h is shown in Fig. 24 to Fig. 27, respectively. The cross sections of the oxide surface after 500 h and 5000 h of exposure with and without cathode contact are shown in Fig. 28 to Fig. 31. The oxide layers appear to grow approximately to thickness of 3 µm with and 3.5 µm without cathode contact during 5000 h exposure. The appearance of the contact area of the cell is shown in Fig. 32 to Fig. 35. Element maps of Si, Cr, Fe and Al for the ZMG 232 surface cross section after 5000 h in contact (also including O and Mn) and outside contact to the cell cathode are shown in Fig. 36 to Fig. 39. Al content is highest (16-22%) below the Cr rich oxide, as a discontinuous layer with a maximum thickness of about 3 µm. Silicon content is highest in a thin (about 1-2 µm) and almost continuous layer between the Cr rich and Al rich oxides. Otherwise the oxide includes a continuous distribution of the expected principal cations of Cr (30-50%) and Mn (22-25%). Fe content of the oxide is about 2-8%. There is practically no difference between the oxides with and without cathode contact in terms of

observed composition. After 5000 h, the contact areas of the cell cathode exhibit local lighter regions which in EDS analysis show elevated chromium content of about 20% (Fig. 40). No chromium was observed outside the lighter regions or after annealing times up to 50 h.

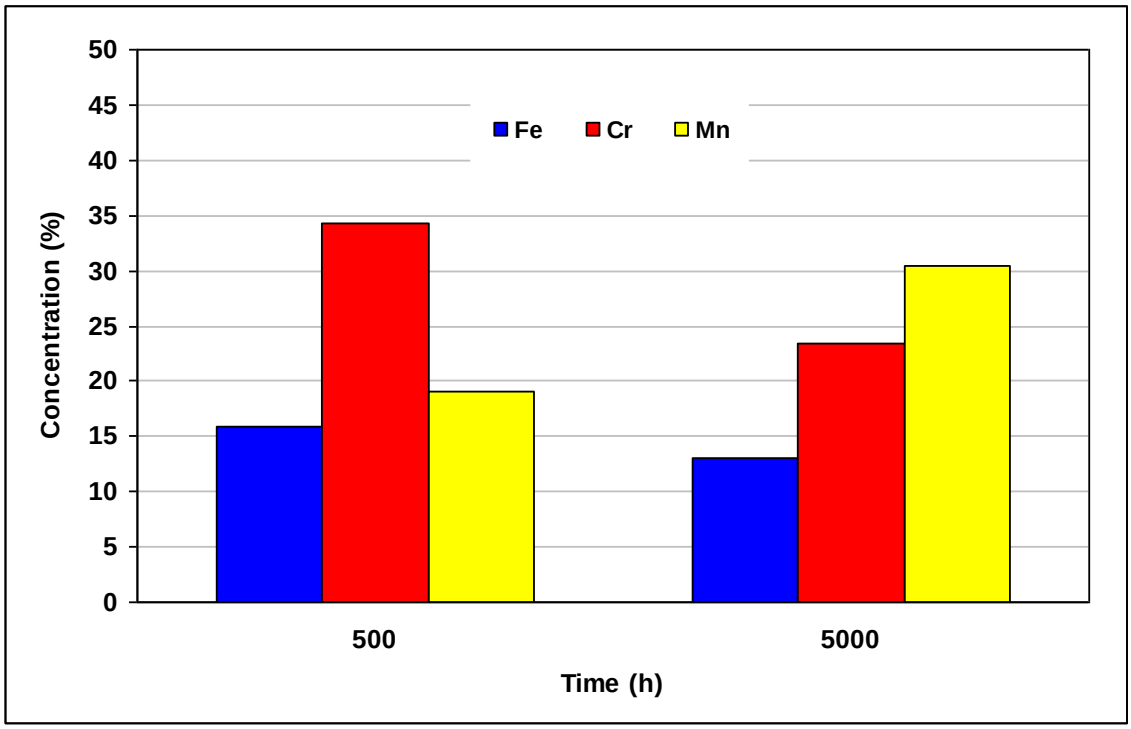

Fig. 23. Observed change in concentration of selected elements on the surface of ZMG 232 during annealing at 740°C in contact with the cathode side of a SOFC cell (EDS analysis).

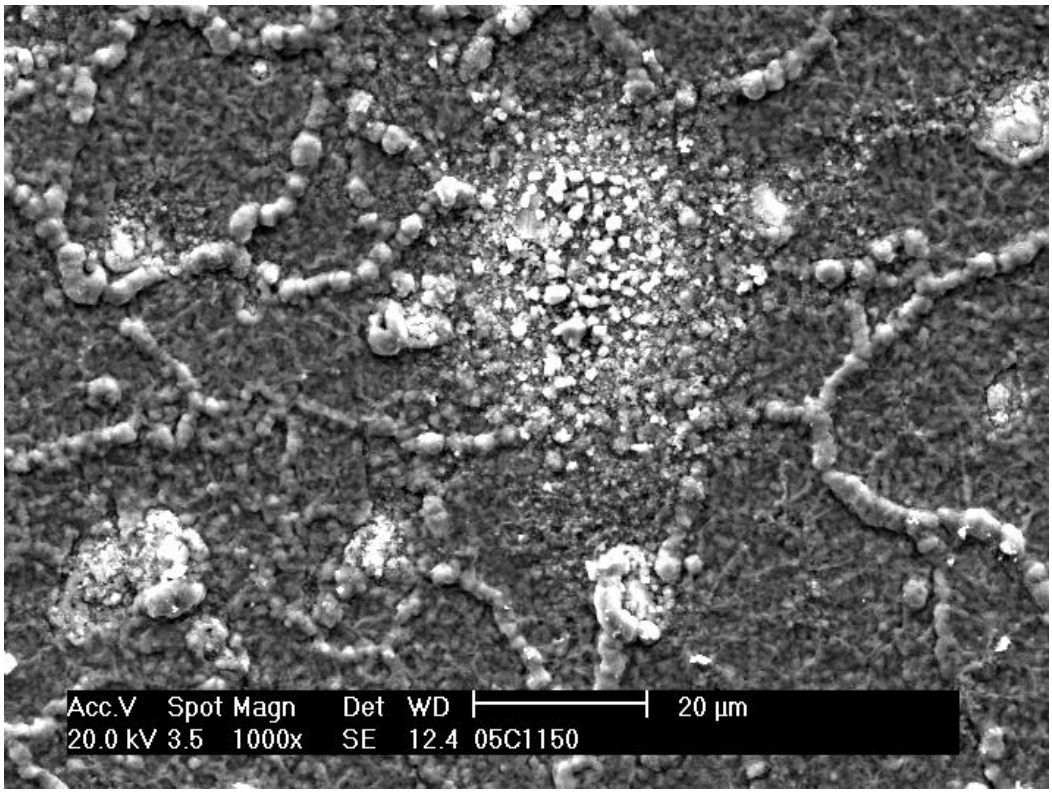

Fig. 24. Surface appearance of ZMG 232 after 500 h at 740°C in contact with SOFC cell cathode.

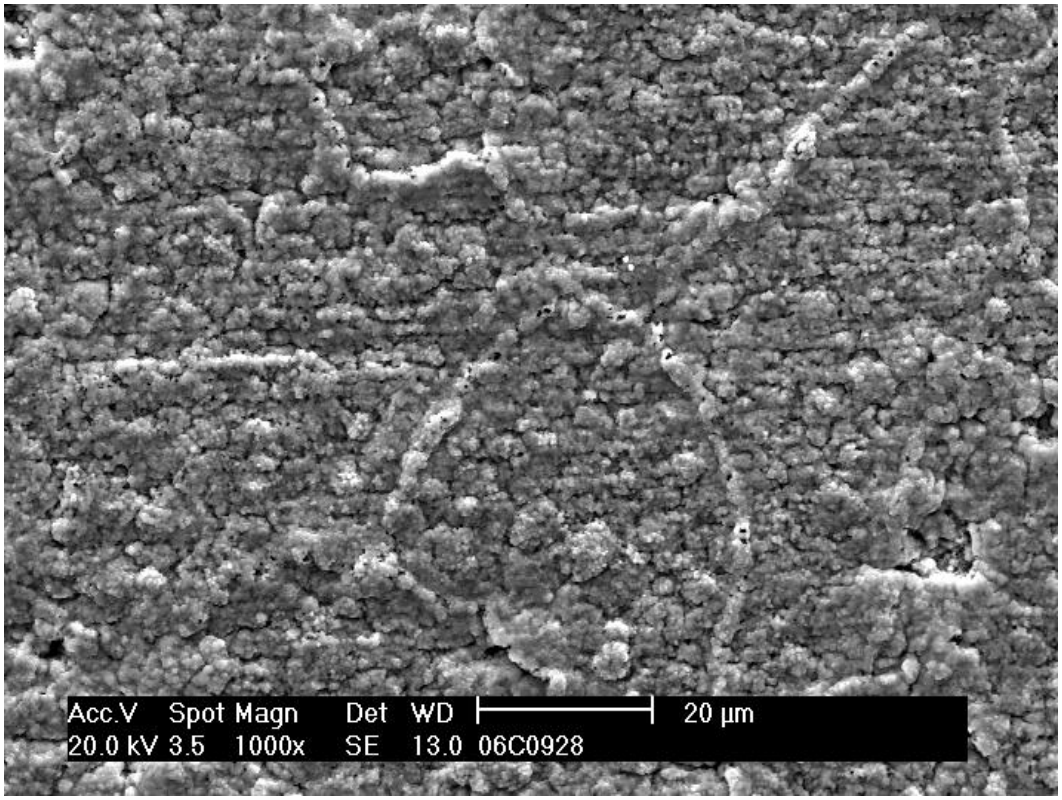

Fig. 25. Surface appearance of ZMG 232 after 5000 h at 740°C in contact with SOFC cell cathode.

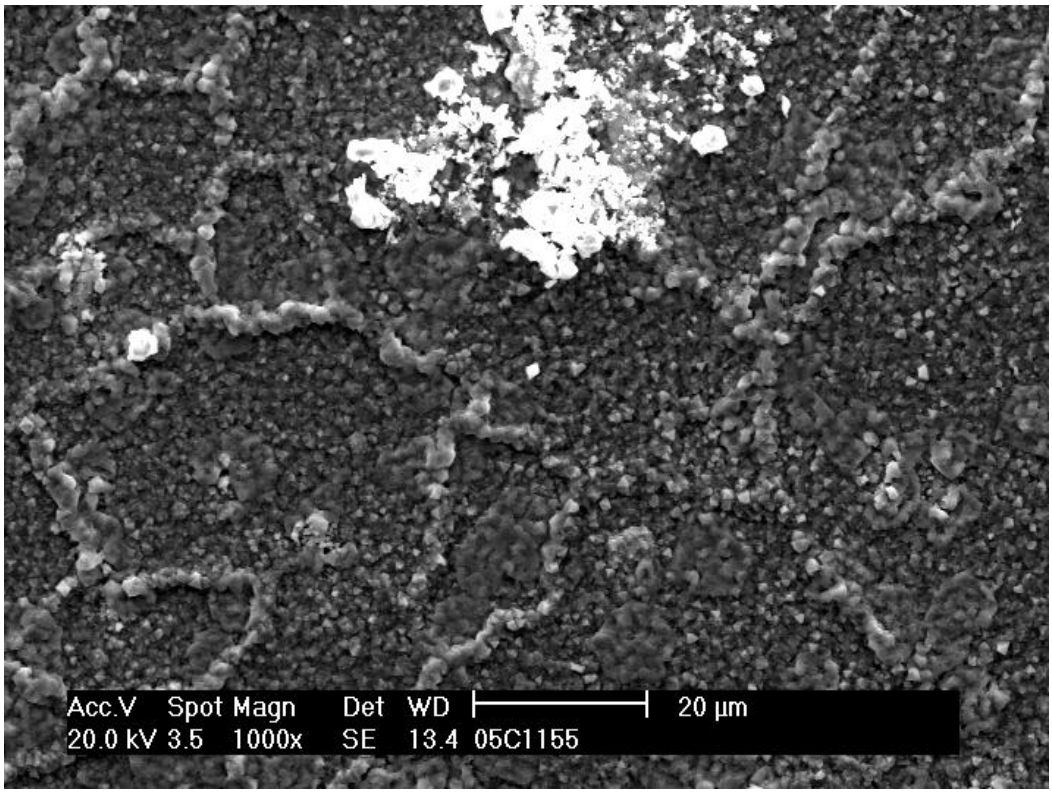

Fig. 26. Surface appearance of ZMG 232 after 500 h at 740°C outside cell contact.

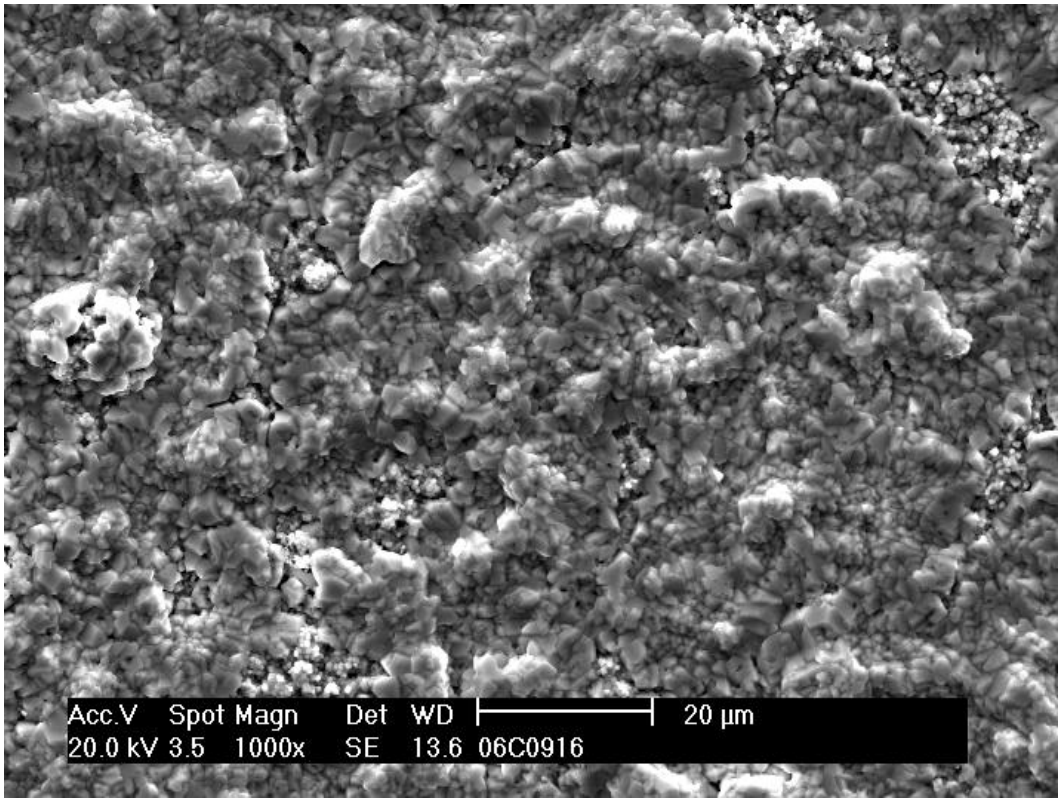

Fig. 27. Surface appearance of ZMG 232 after 5000 h at 740°C outside cell contact.

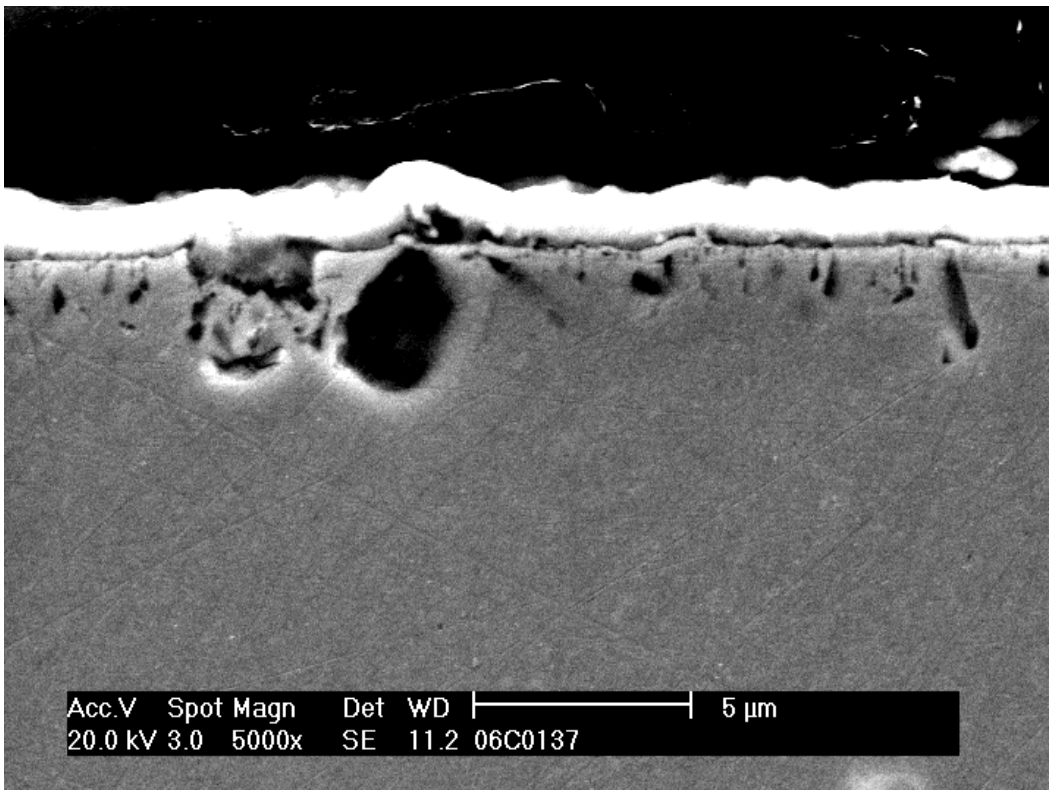

Fig. 28. Cross-section of ZMG 232, after 500 h at 740°C in cathode contact.

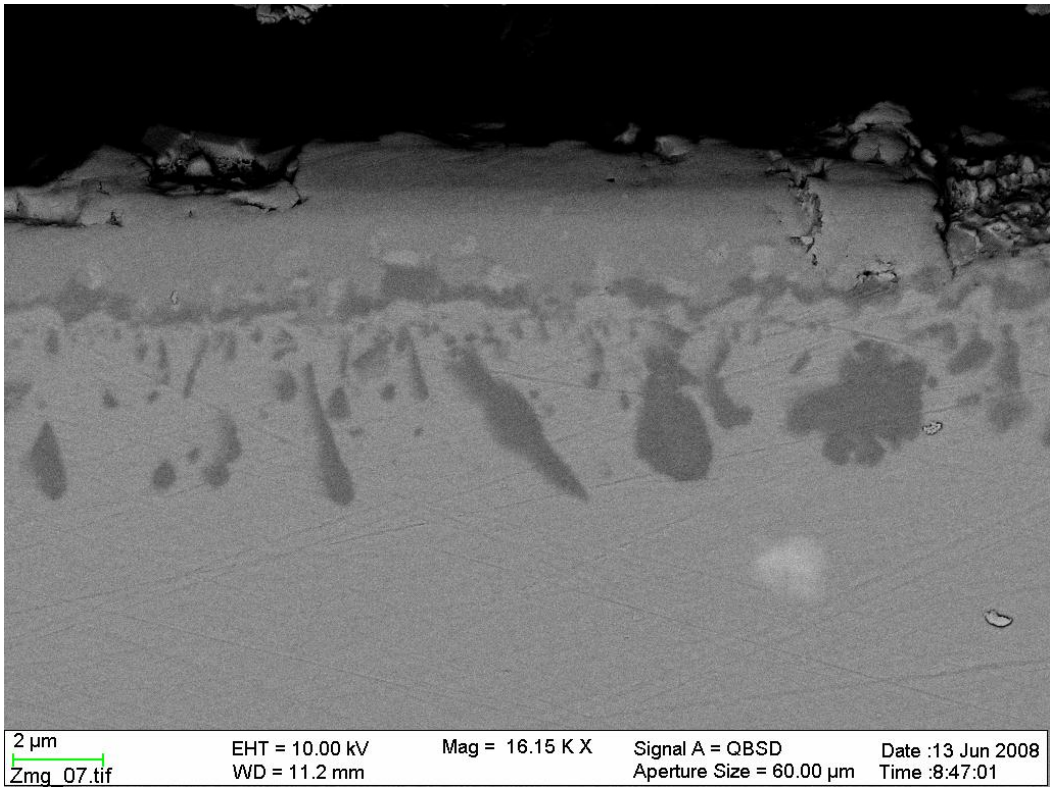

Fig. 29. Cross-section of ZMG 232, after 5000 h at 740°C in cathode contact.

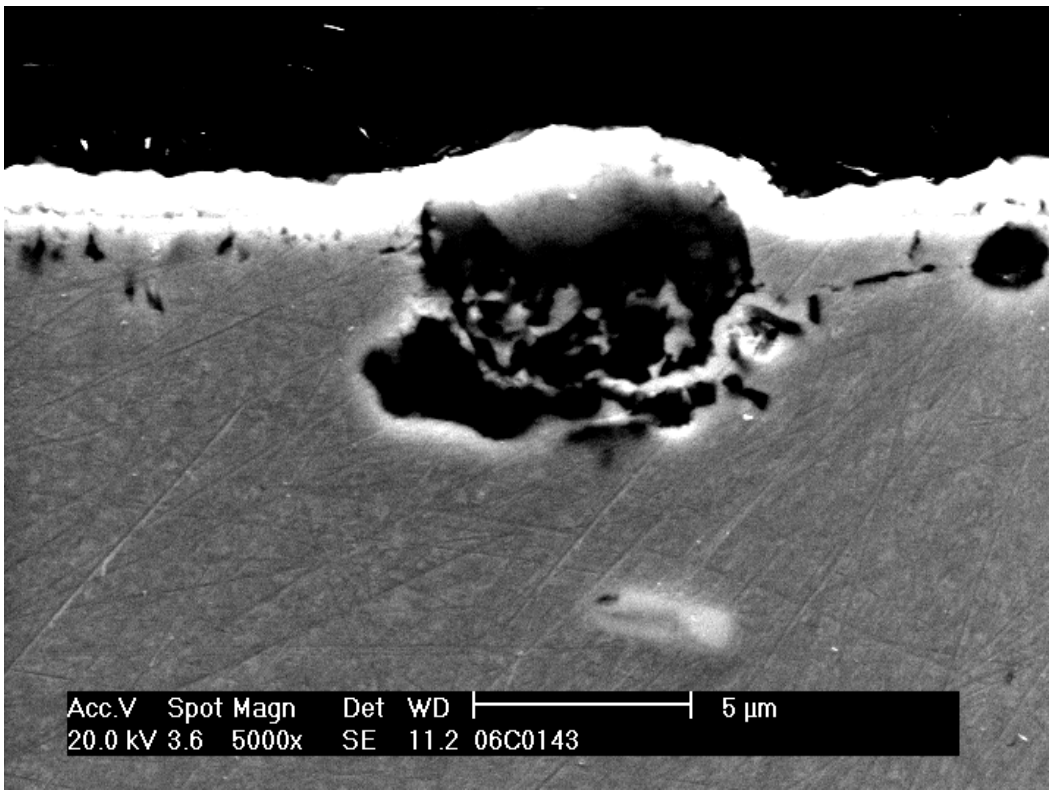

Fig. 30. Cross-section of ZMG 232, after 500 h at 740°C outside cathode contact.

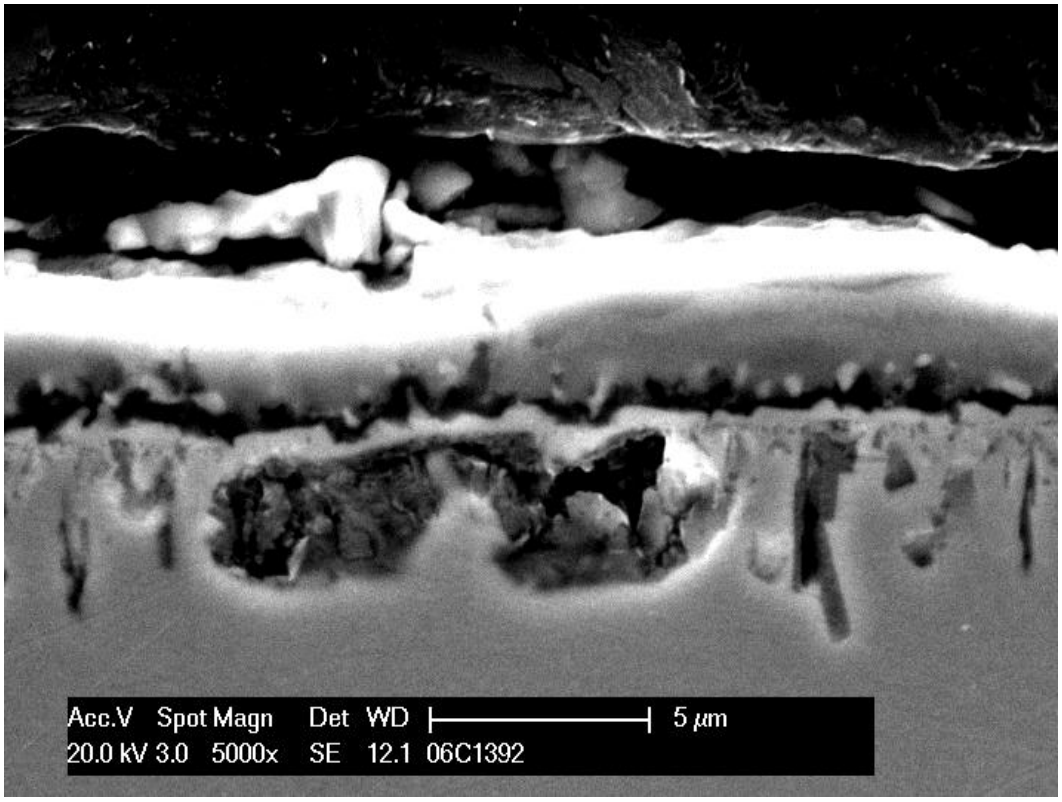

Fig. 31. Cross-section of ZMG 232, after 5000 h at 740°C outside cathode contact.

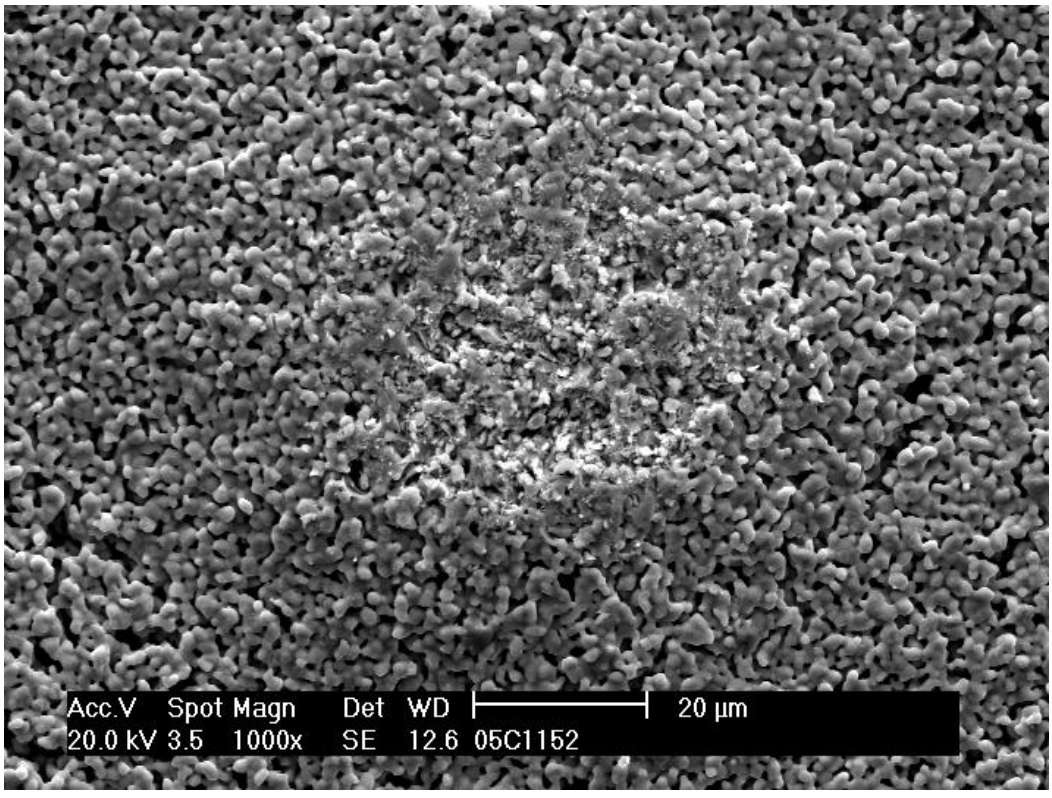

Fig. 32. The appearance of the cathode side cell surface after 500 h at 740°C in contact with ZMG 232.

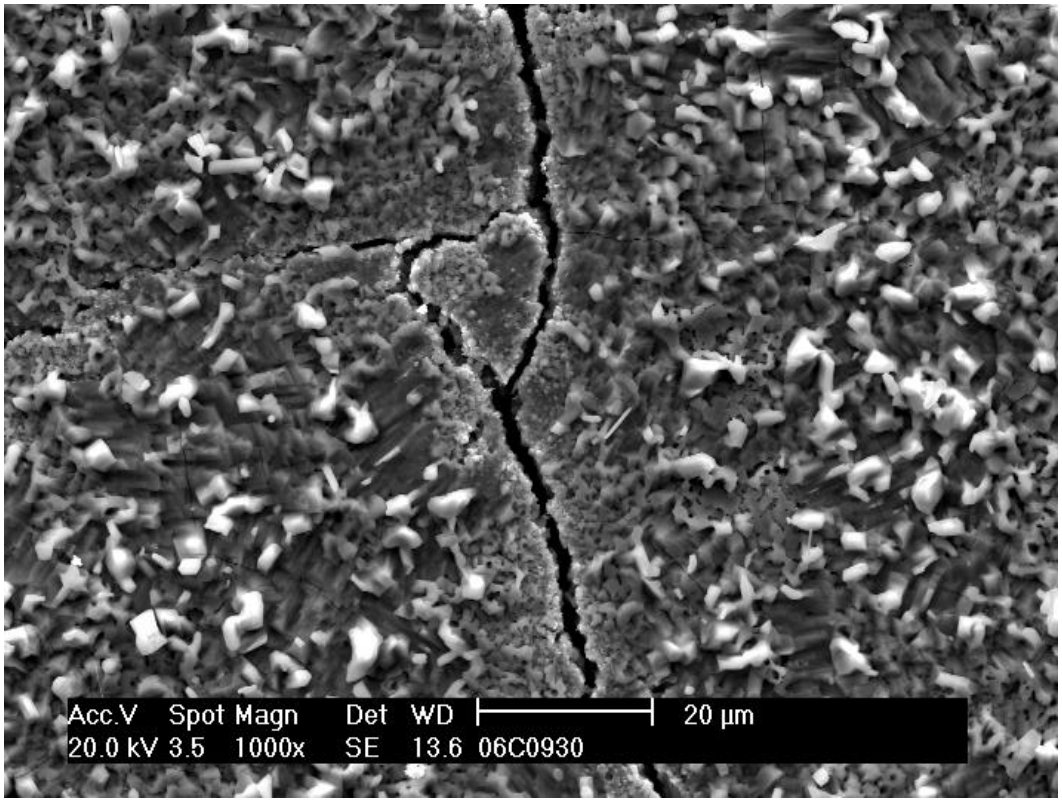

Fig. 33. The appearance of the cathode side cell surface after 5000 h at 740°C in contact with ZMG 232.

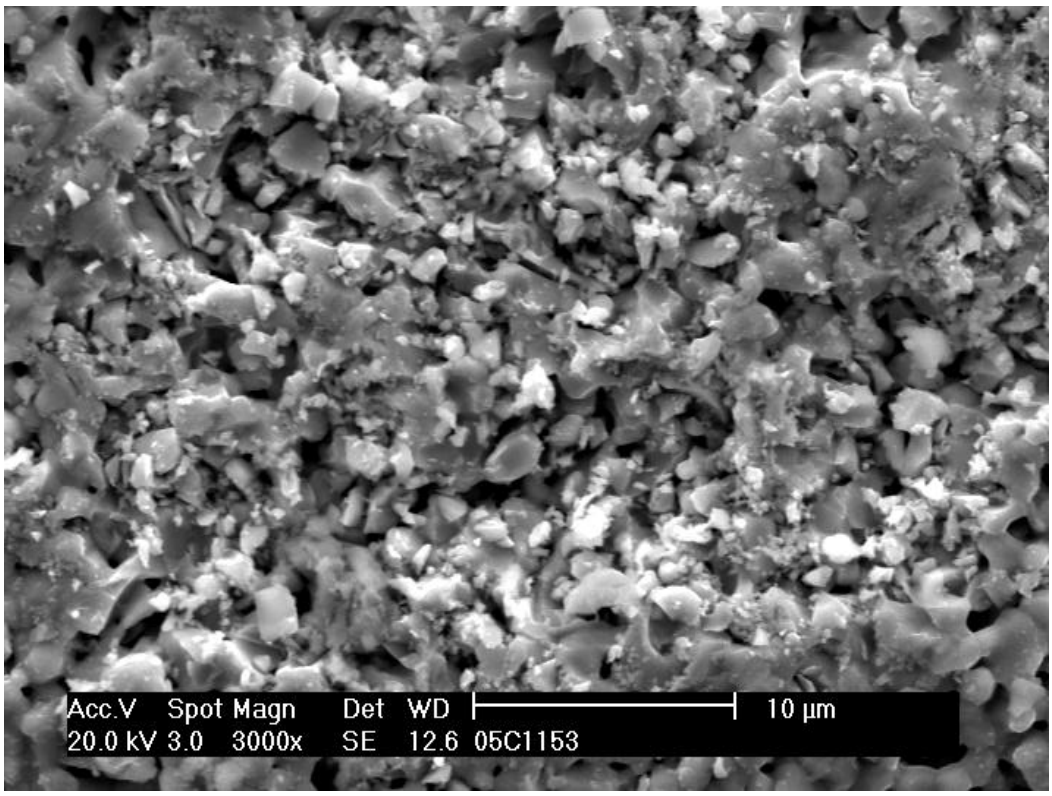

Fig. 34. Partial magnification of the lighter region of Fig. 32, suggesting possible contact and contamination from the bipolar plate alloy (500 h).

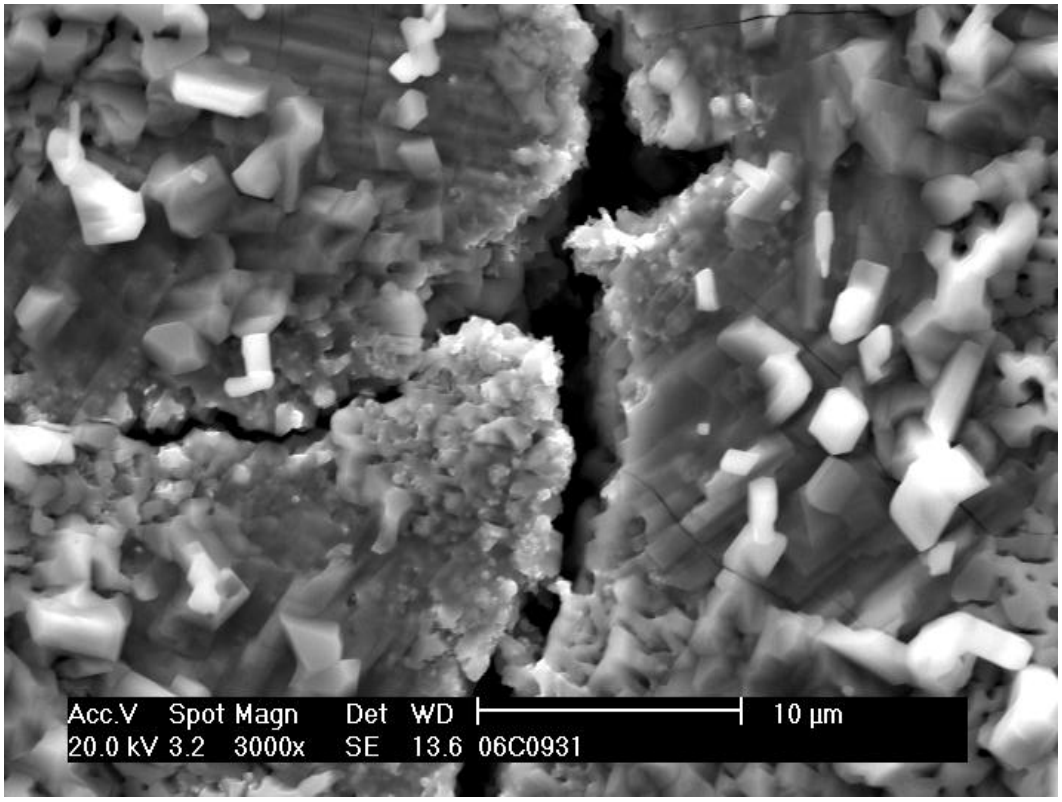

Fig. 35. Partial magnification of the lighter region of Fig. 33, suggesting possible contact and contamination from the bipolar plate alloy (5000 h).

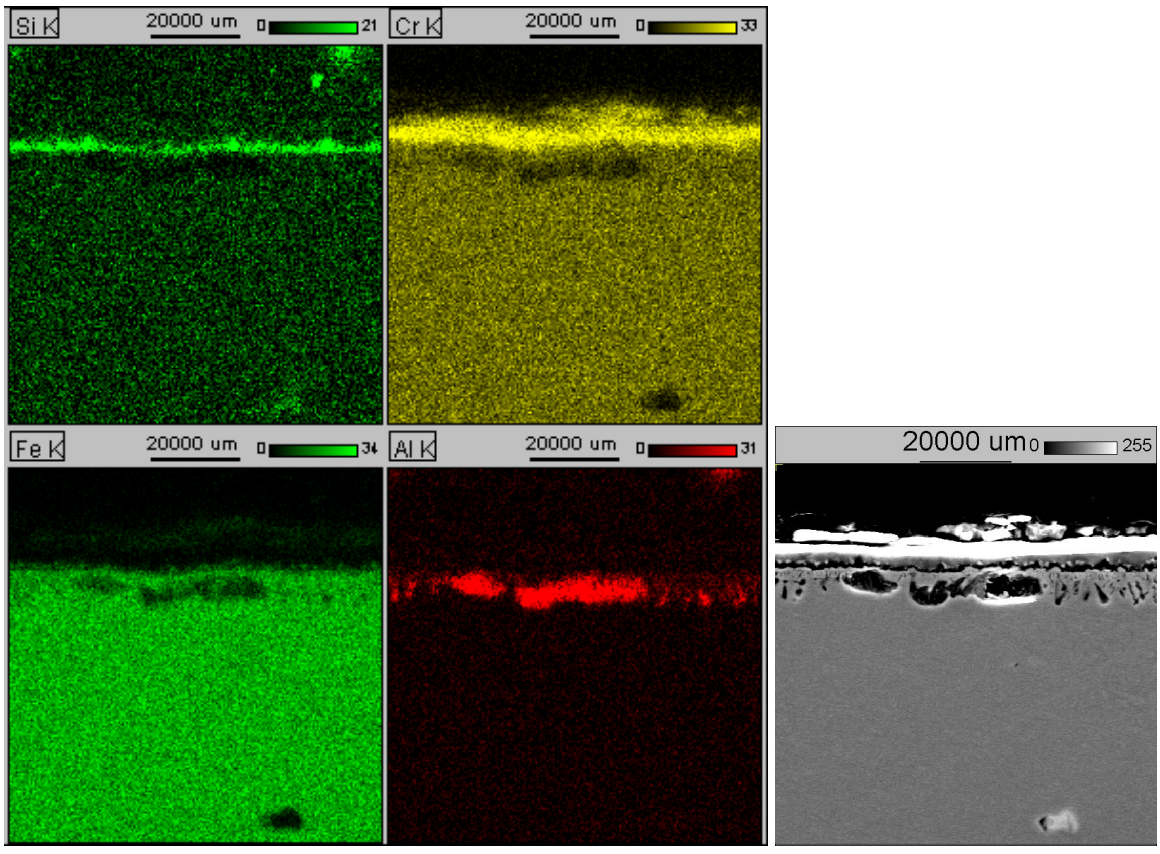

Fig. 36. Element maps of Si, Cr, Fe and Al for the ZMG 232 surface after 5000 h of exposure (outside cathode contact); actual scale 10µm.

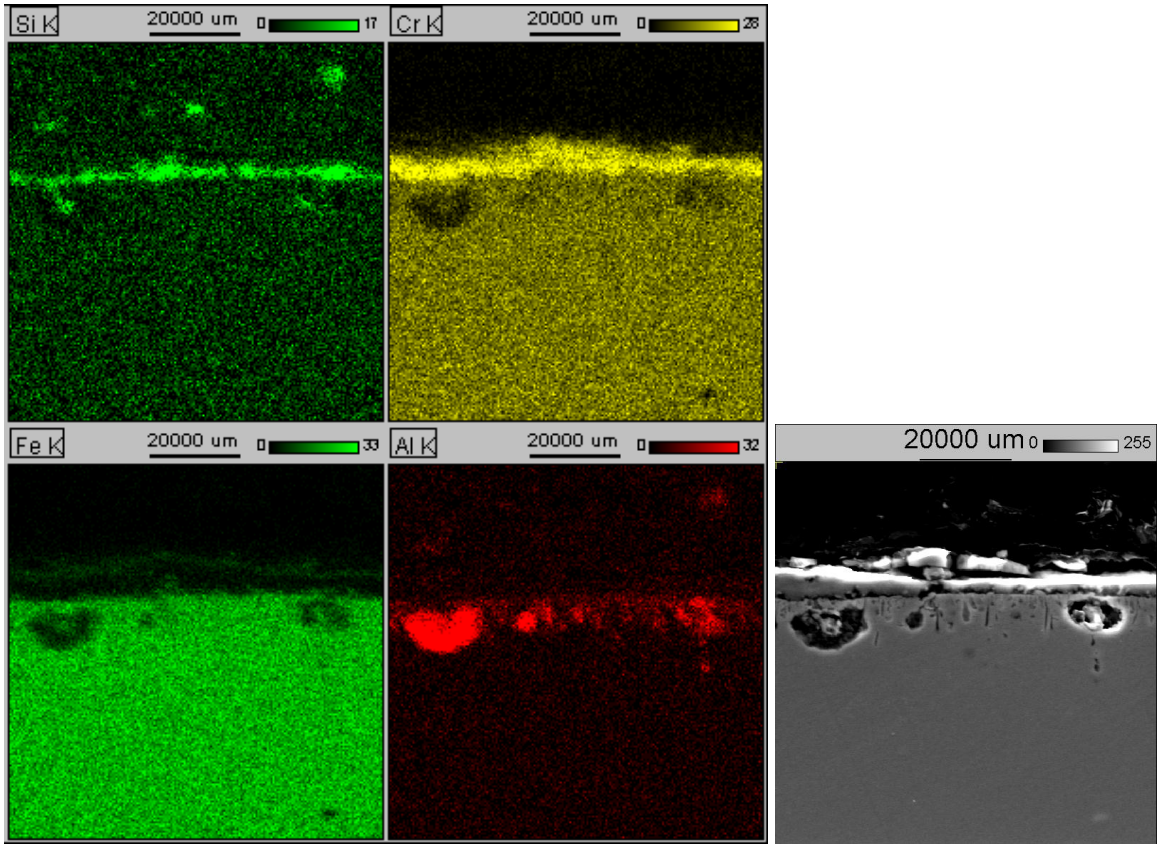

Fig. 37. Element maps of Si, Cr, Fe and Al for the ZMG 232 surface after 5000 h of exposure (cathode contact); actual scale 10 µm.

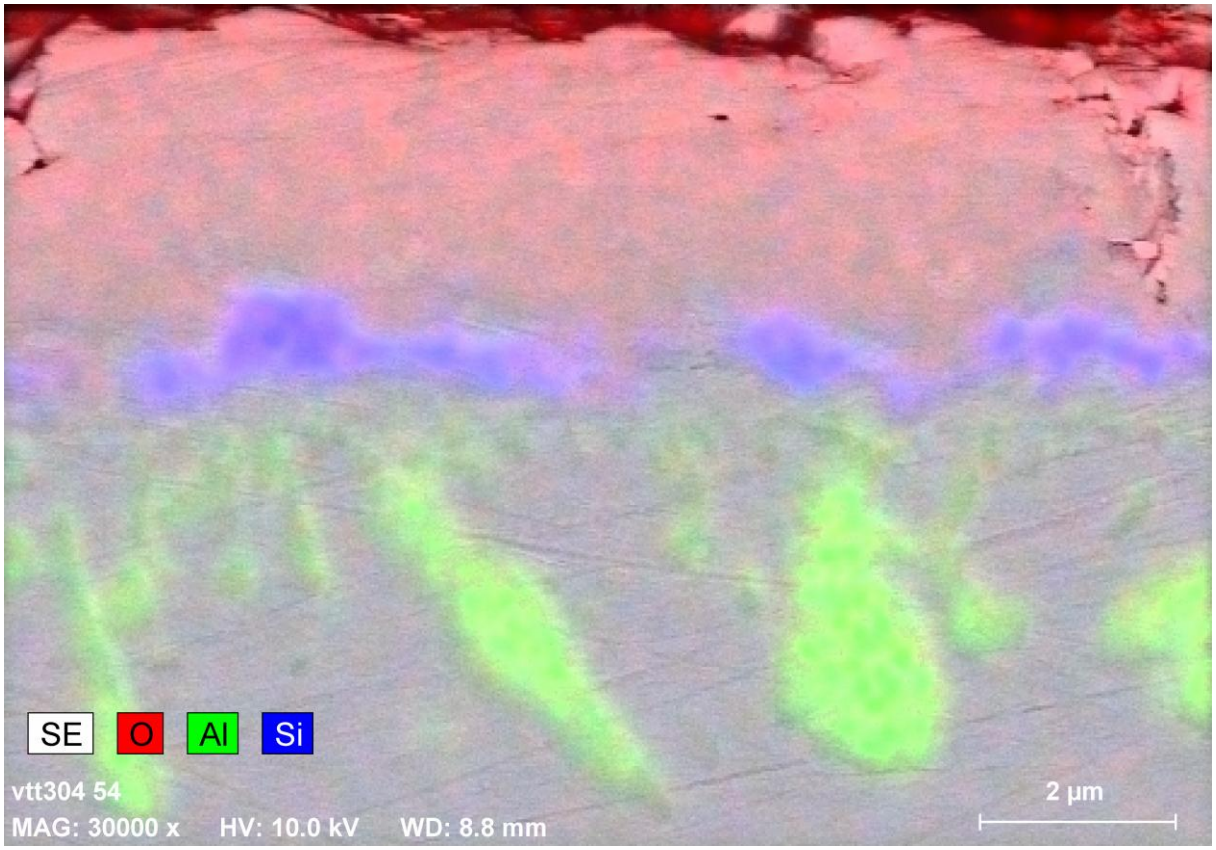

Fig. 38. Element map of O, Al and Si for the ZMG 232 surface cross section after 5000 h of exposure (cathode contact).

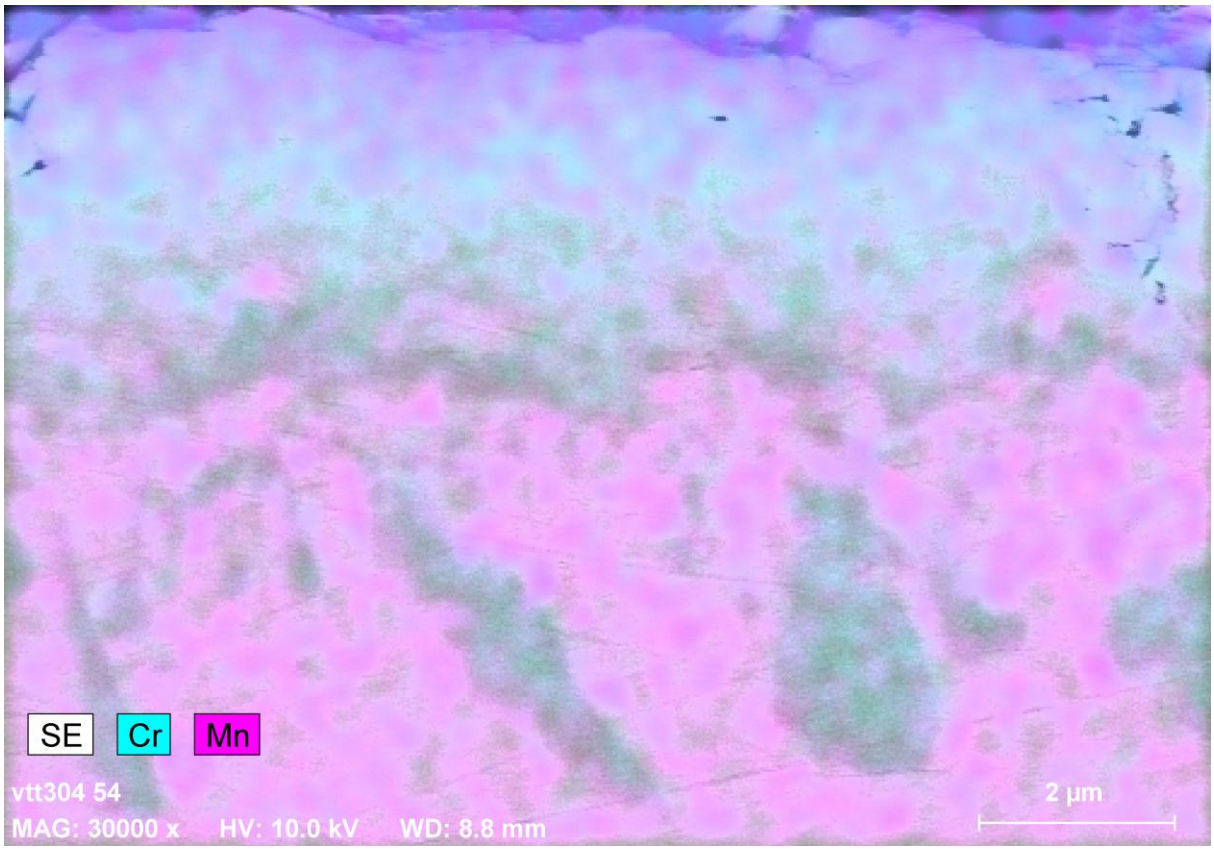

Fig. 39. Element map of Cr and Mn for the ZMG 232 surface cross section after 5000 h of exposure (cathode contact).

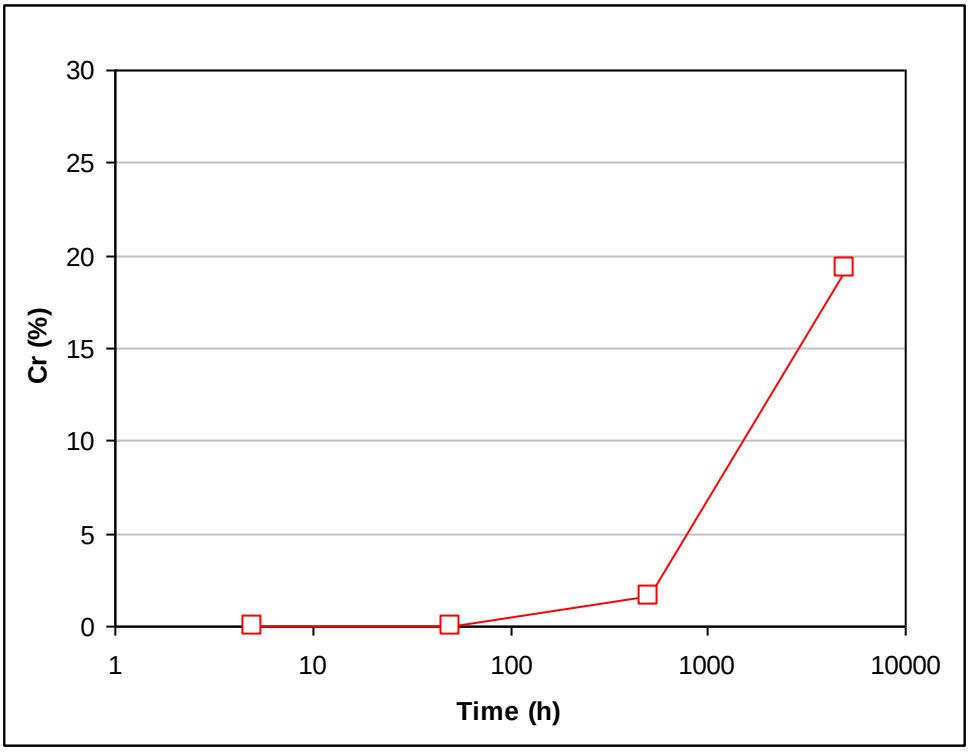

Fig. 40. The chromium content on the contact surface of the SOFC cell (with ZMG 232, EDS analysis).

3.3.2 Microstructural evolution of ZMG 232

The effect of exposure at 740°C on the microstructures of ZMG 232 is shown in Fig. 41 to Fig. 43 for the initial state and after 500 and 5000 h. It can be seen that at this level of detail, the main change of the microstructure is limited to grain growth and possible modification in the carbide structure. In comparison with alloy 430, the microstructure of ZMG 232 includes a less dense distribution of inclusions (carbides); however the largest inclusions are clearly larger in size than in alloy 430.

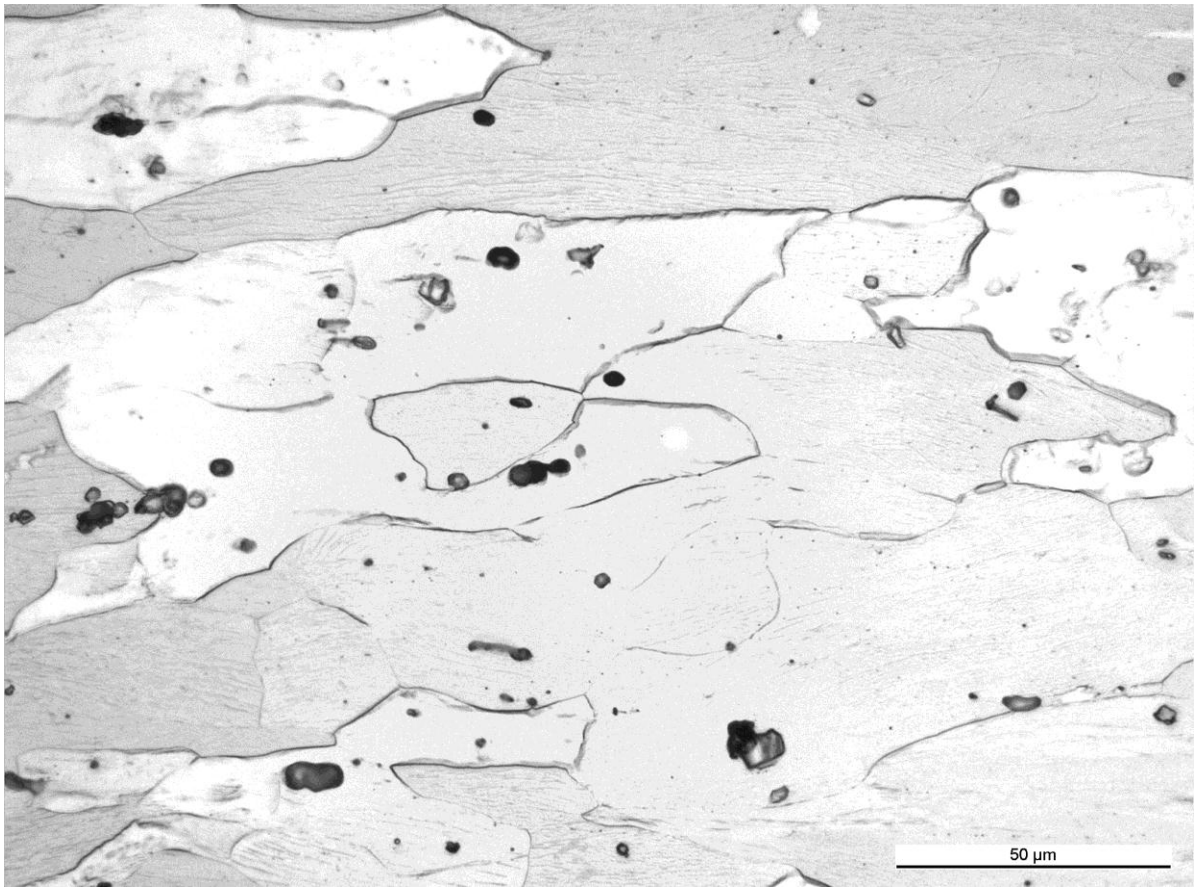

Fig. 41.The microstructure of alloy ZMG 232 as received.

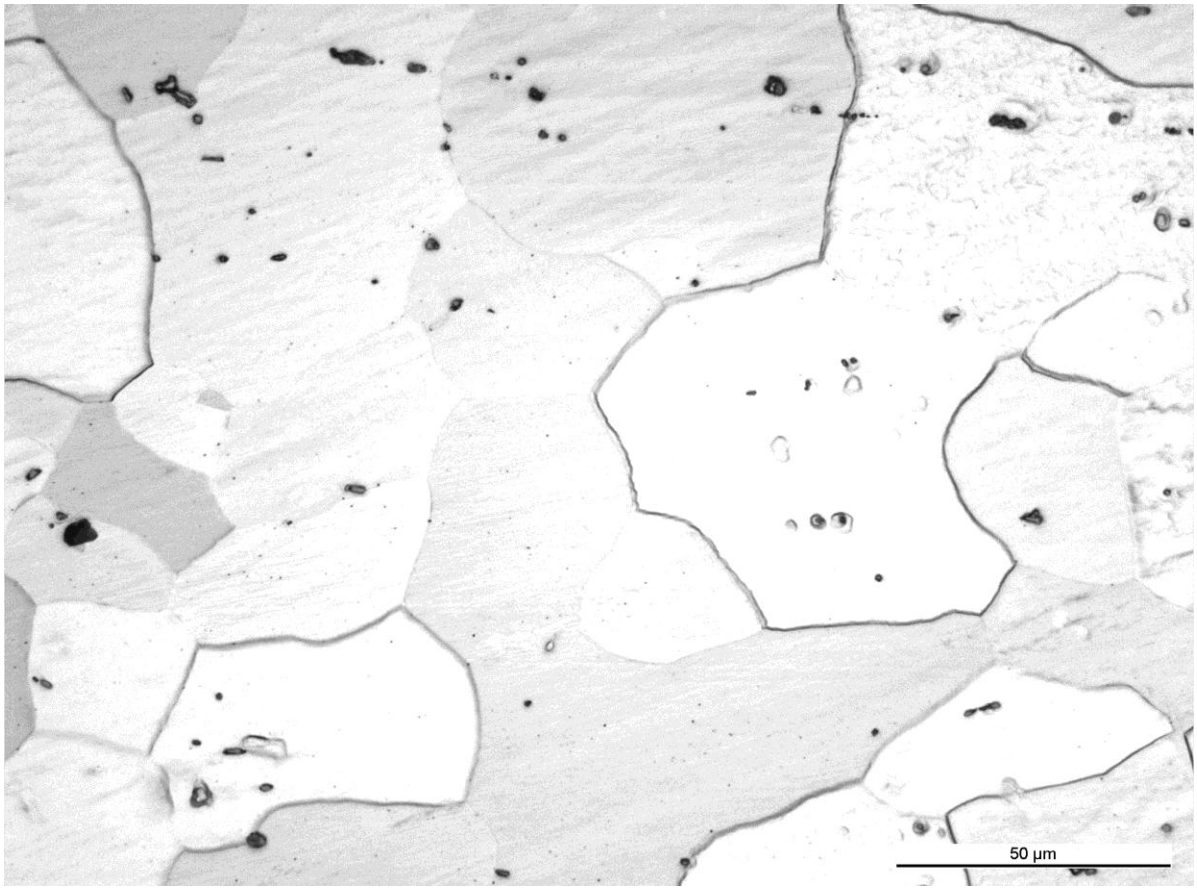

Fig. 42. The microstructure of alloy ZMG 232 after 500 h of exposure.

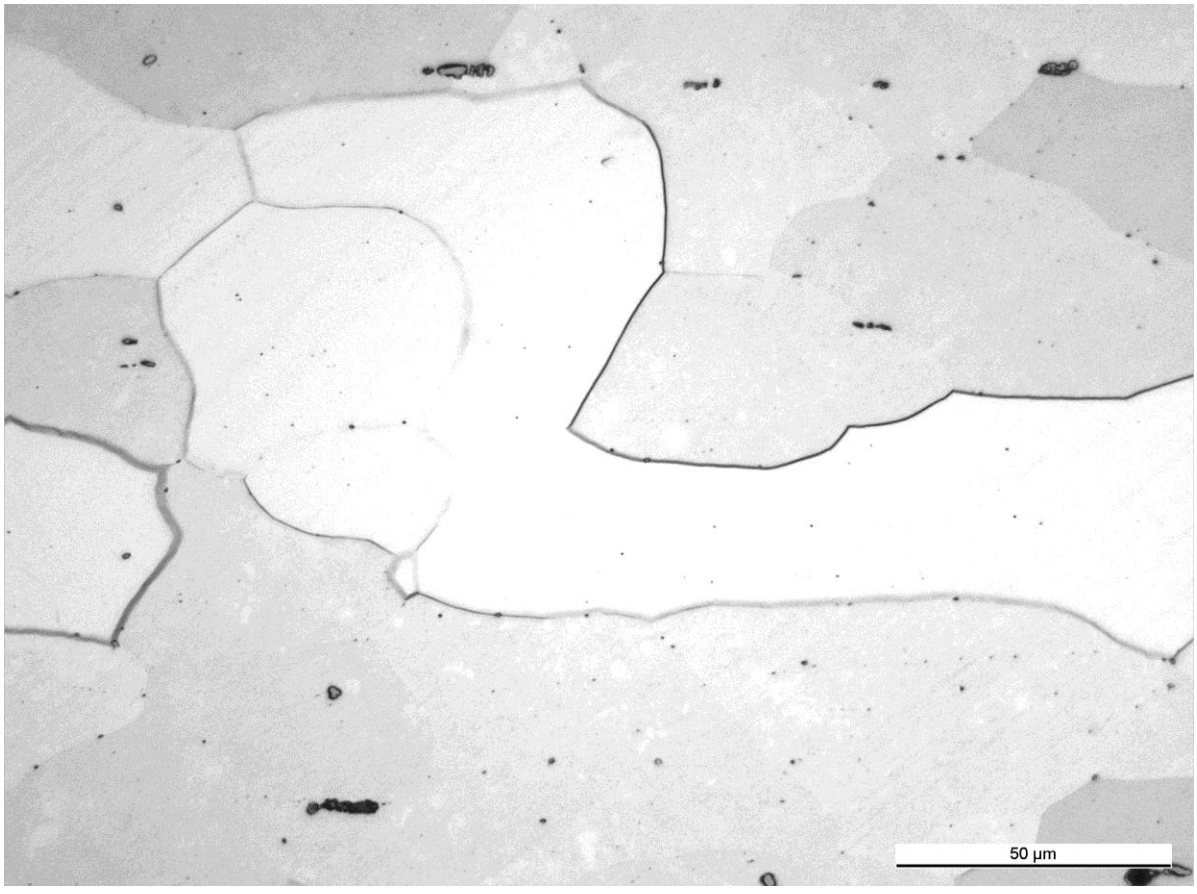

Fig. 43. The microstructure of alloy ZMG 232 after 5000 h of exposure.

3.4 Degradation of Crofer 22 APU

3.4.1 Contact surfaces of Crofer 22 APU

The surface composition of Crofer 22 APU is shown in Fig. 44 after testing in contact with the cell. Increasing Mn content, clearly decreasing Fe content and stable Cr content are seen on these surfaces. At 5000 h the surface Cr content has stabilised to about 40% and Fe content has decreased to about 3% (Fig. 44). No significant difference was observed in the surface compositions within and outside the contact to the cell. The appearance of the metal surfaces within and outside the contact area to the cell after 500 and 5000 h is shown in Fig. 45 to Fig. 48. The cross sections of the oxide surface after 500 and 5000 h of exposure with and without cathode contact are shown in Fig. 49 to Fig. 52. The oxide has grown to a thickness of about 3 µm with and 2 µm without cathode contact for 5000 h. The appearance of the contact area of the cell is shown in Fig. 53 and Fig. 54. Element maps of Si, Cr, Fe and Al for the Crofer 22 APU surface cross section after 5000 h in contact (also including O, Ti, Mn and La) and outside contact to the cell cathode are shown in Fig. 55 and Fig. 58. Al and Si are relatively evenly distributed in the base material but are reduced in the oxide; however the local maximum content for both is well below 0.5%. Otherwise the metal oxide includes a continuous layer including the expected principal cations of Cr (40-45%) and Mn (22-31%). Fe content of the oxide is about 4-8%. Some titanium rich precipitates appear in the base material, while in the oxide Ti is fairly evenly distributed with a content of about 0.3-0.5%. There is little difference between the oxides with and without cathode contact in terms of observed composition. After 5000 h, the contact surfaces of the cell cathode showed in EDS analysis an elevated chromium content of about 20% (Fig. 59). In contrast, no chromium was observed on the corresponding cell surfaces after annealing times up to 500 h.

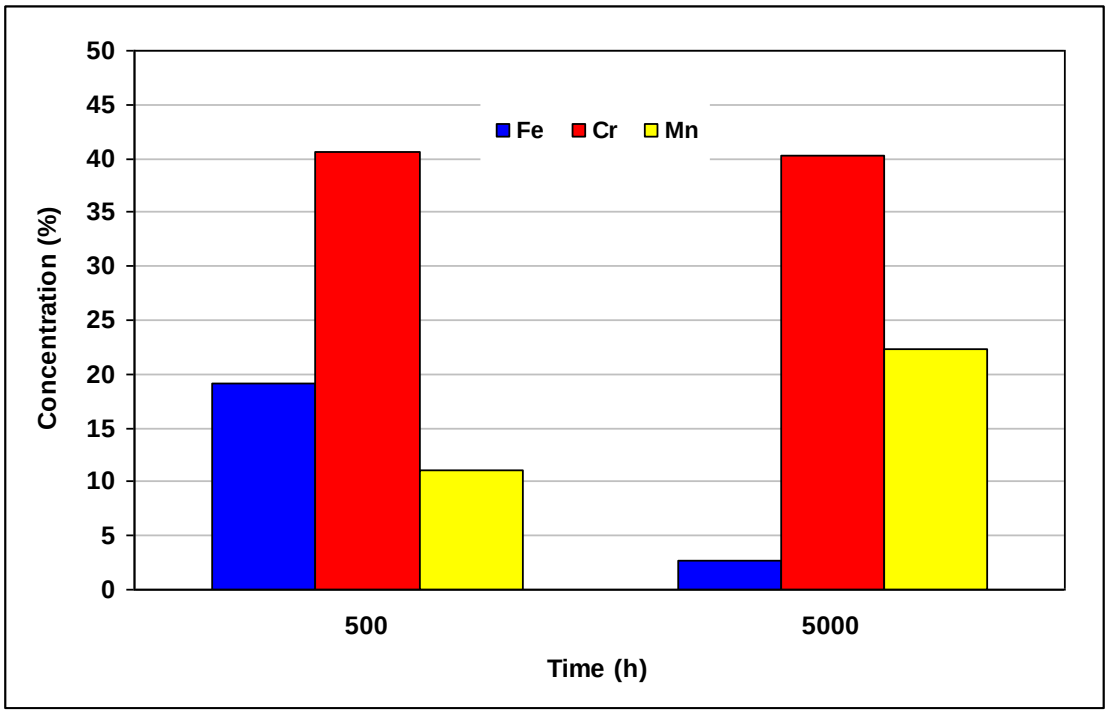

Fig. 44. Observed change in concentration of selected elements on the surface of Crofer 22 APU during annealing at 740°C in contact with the cathode side of a SOFC cell (EDS analysis).

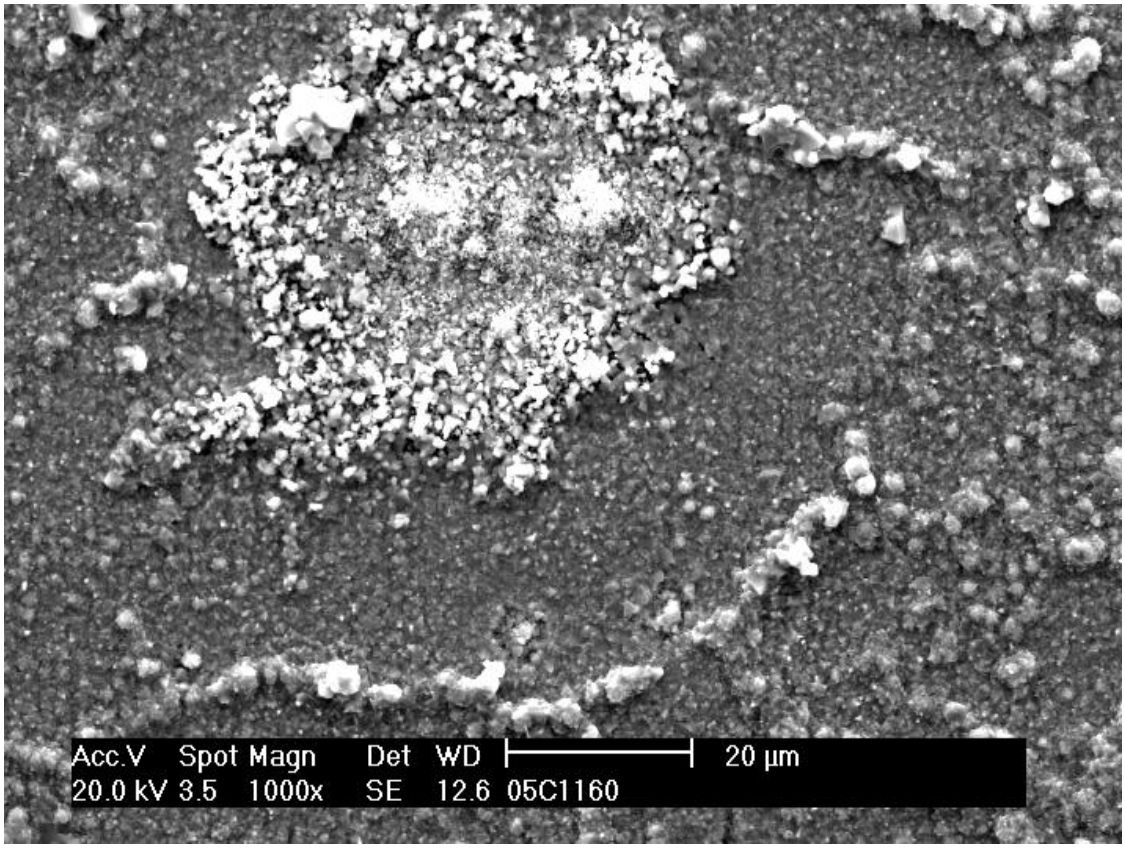

Fig. 45. Surface appearance of Crofer 22 APU after 500 h at 740°C in contact with SOFC cell cathode.

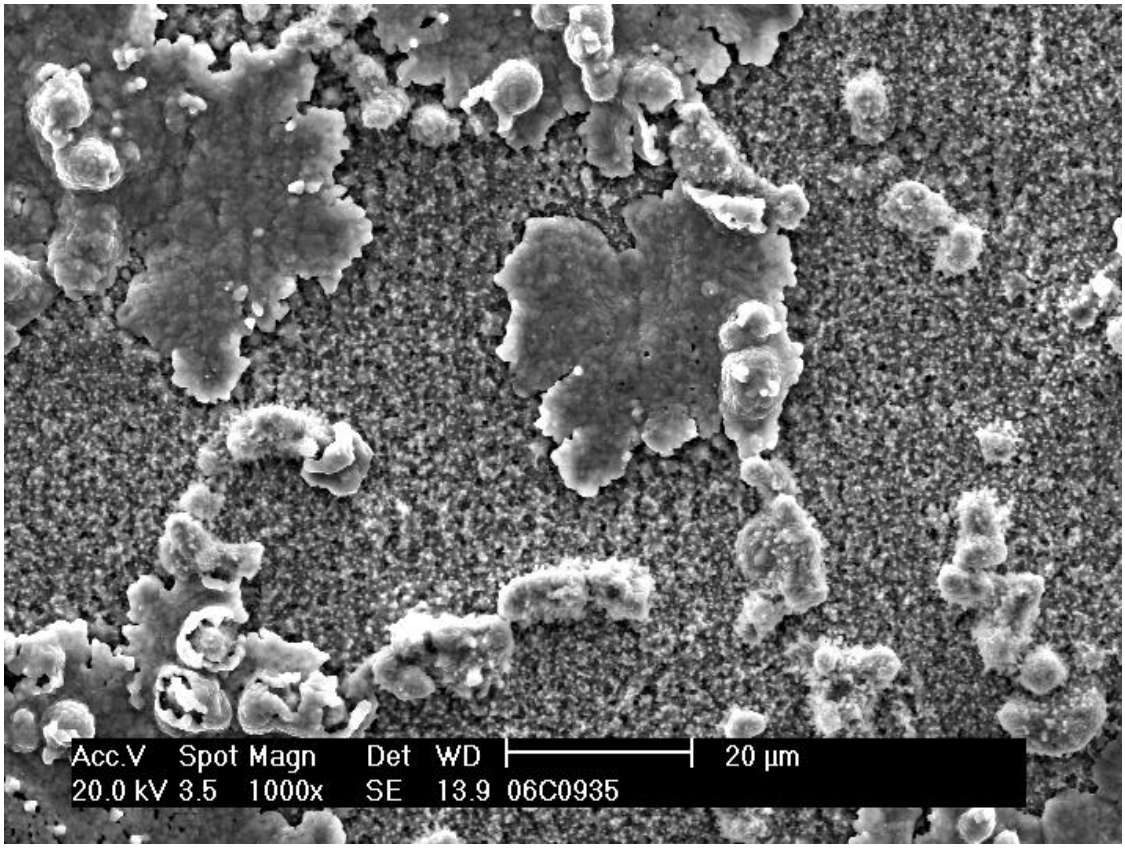

Fig. 46. Surface appearance of Crofer 22 APU after 5000 h at 740°C in contact with SOFC cell cathode.

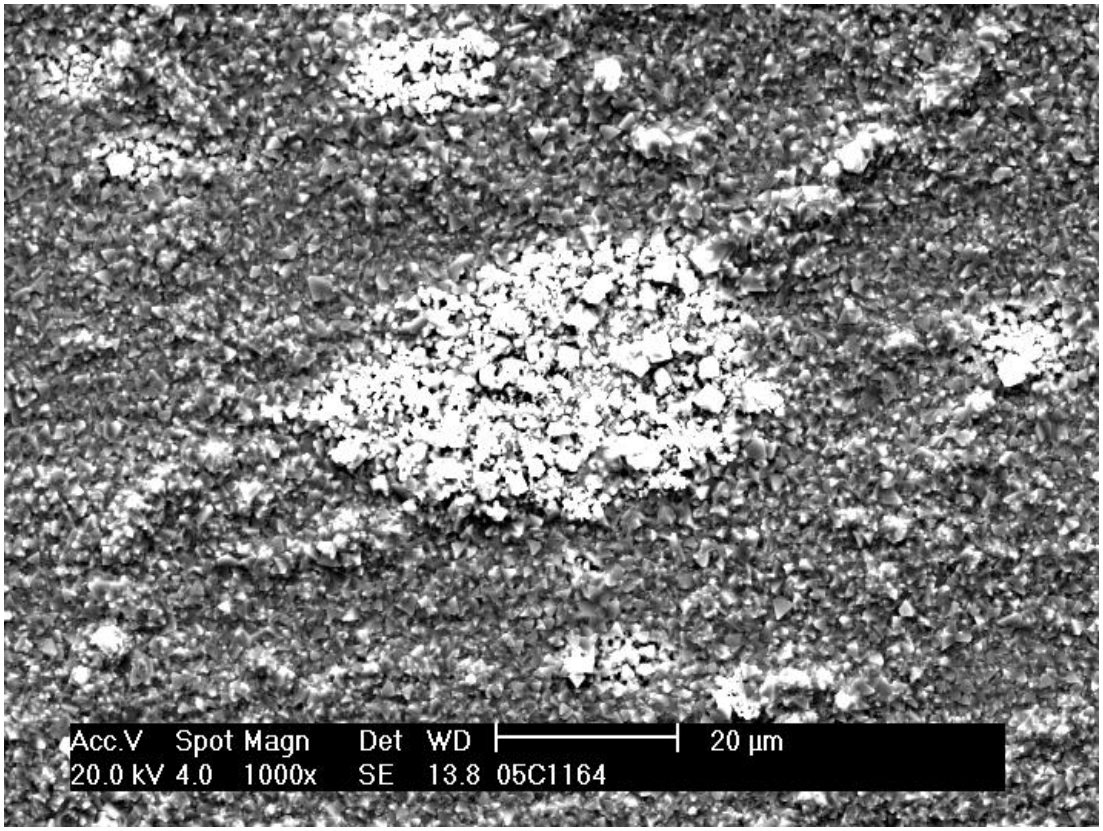

Fig. 47. Surface appearance of Crofer 22 APU after 500 h at 740°C outside cell contact.

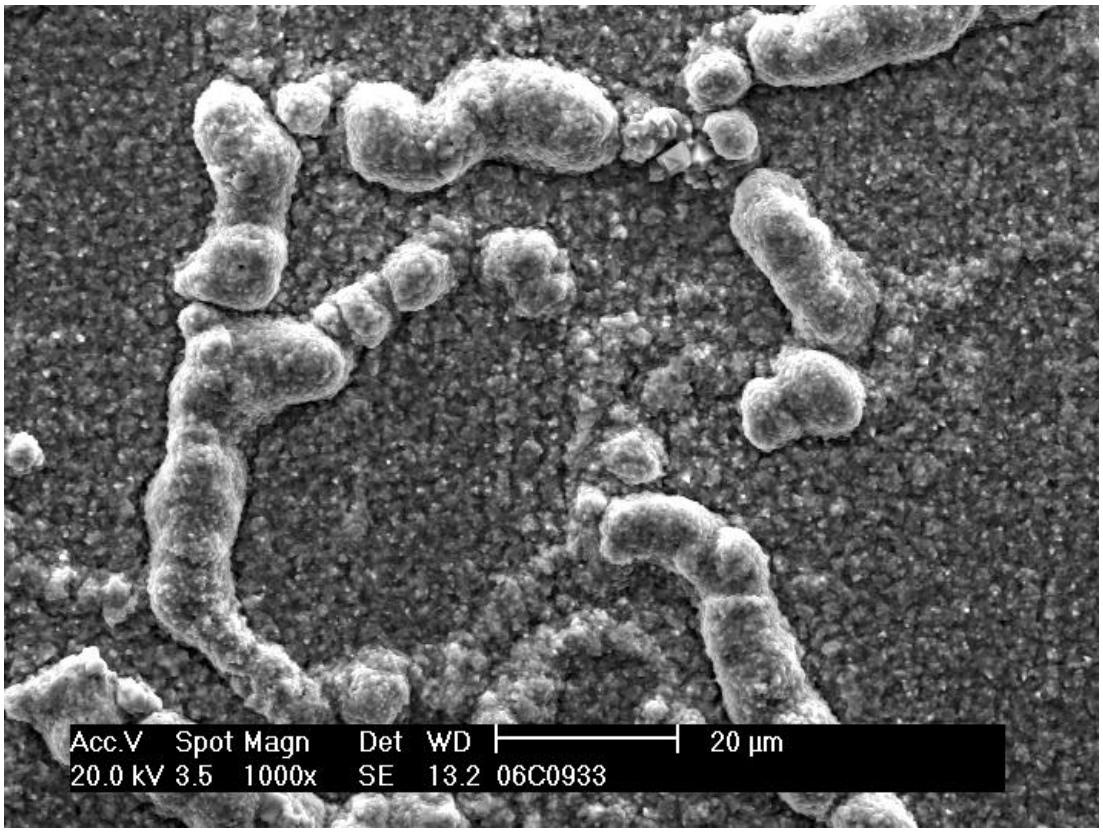

Fig. 48. Surface appearance of Crofer 22 APU after 5000 h at 740°C outside cell contact.

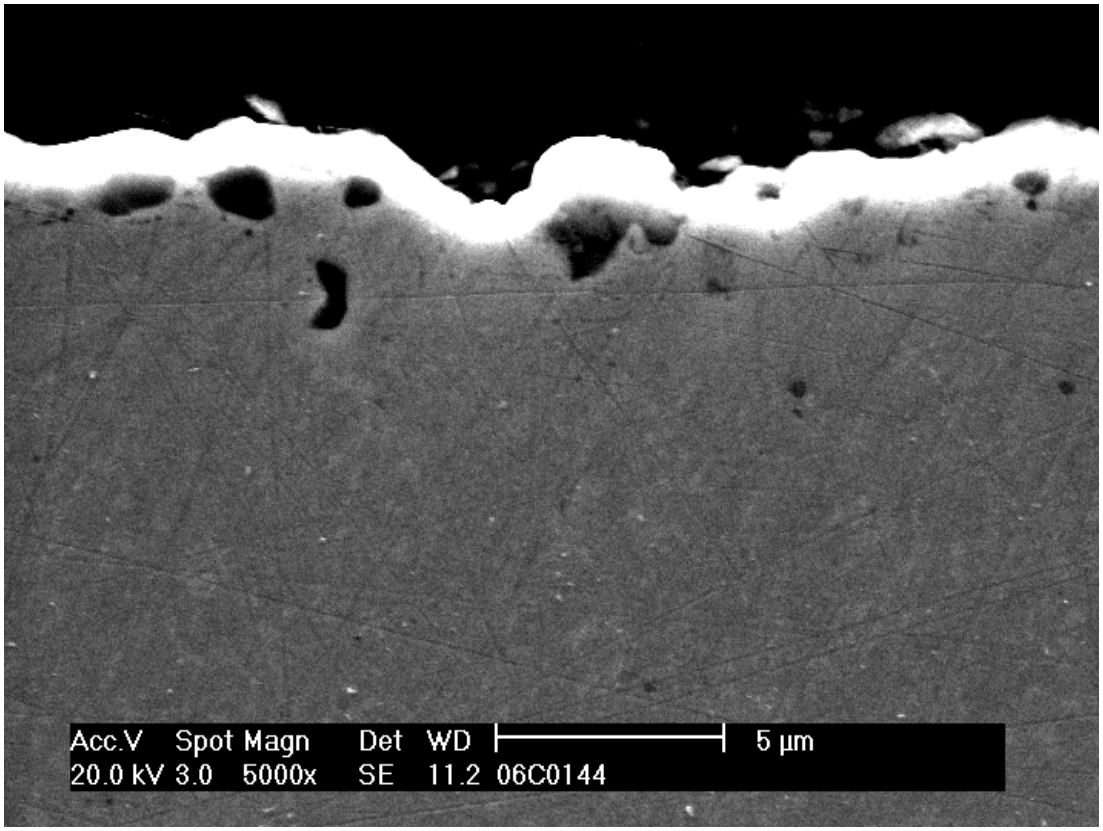

Fig. 49. Cross-section of Crofer 22 APU after 500 h at 740 °C in cathode contact.

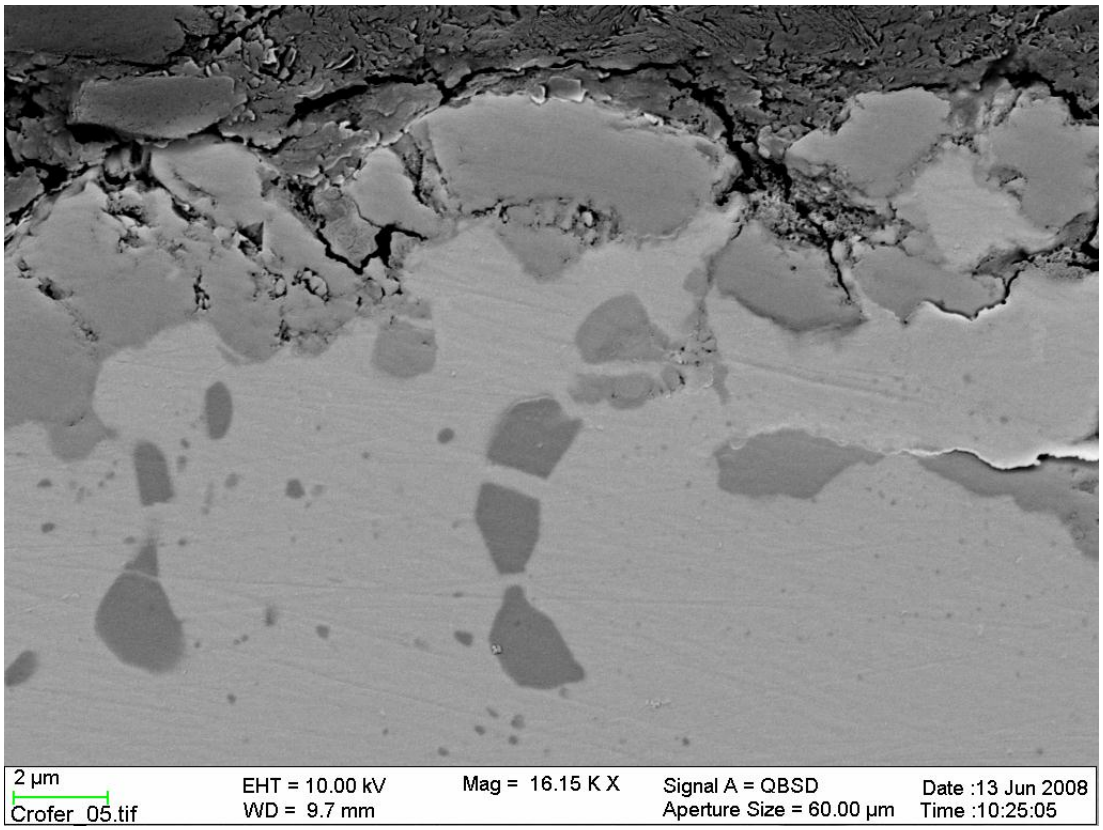

Fig. 50. Cross-section of Crofer 22 APU after 5000 h at 740 °C in cathode contact.

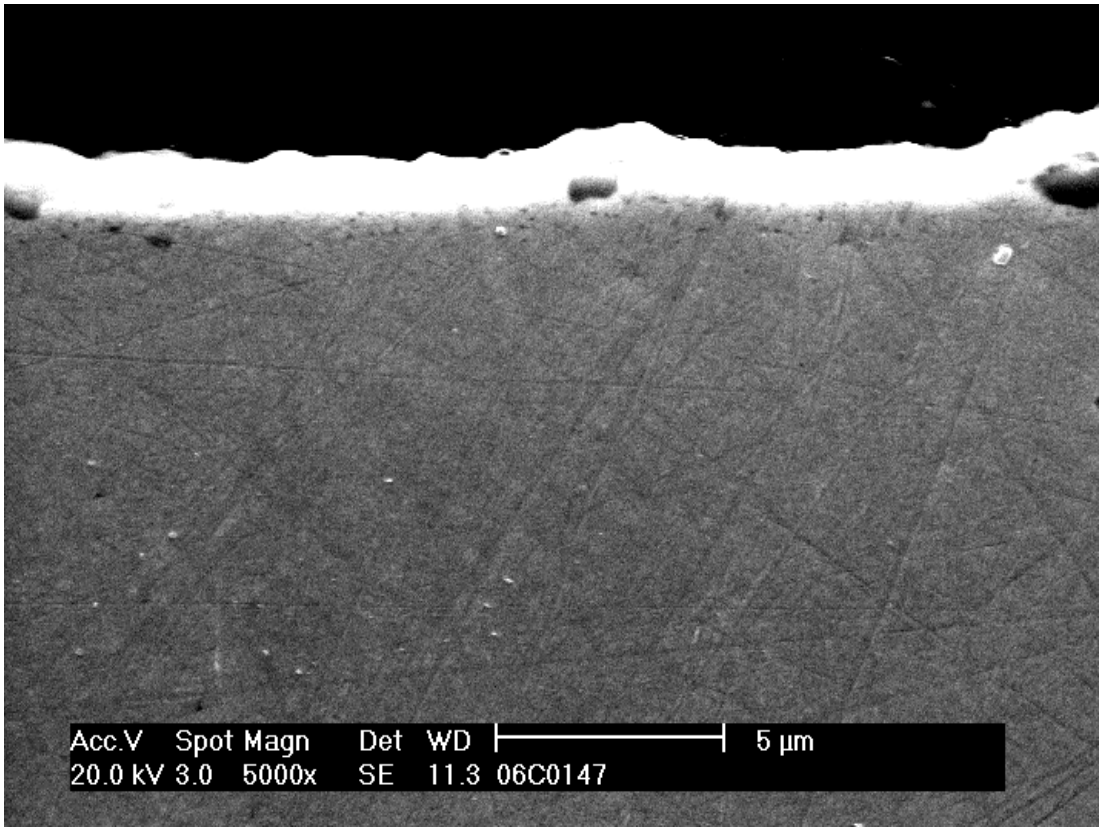

Fig. 51. Cross-section of Crofer 22 APU after 500 h at 740°C outside cathode contact.

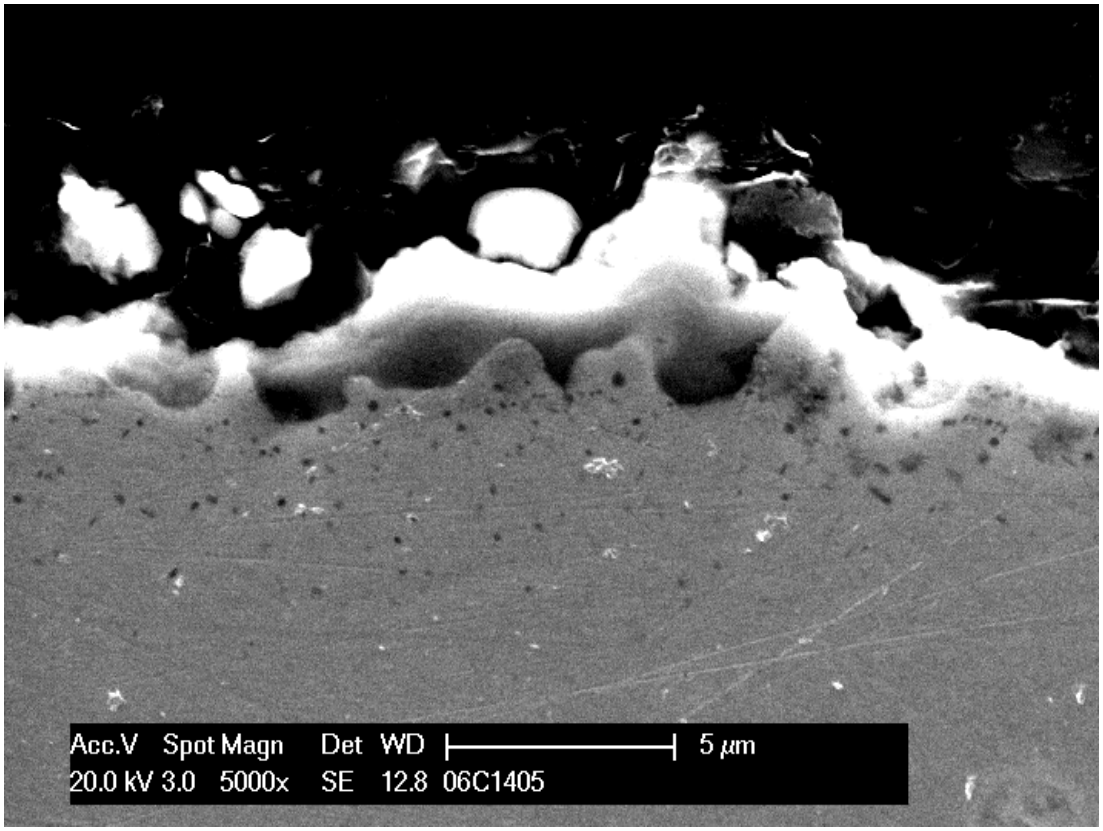

Fig. 52. Cross-section of Crofer 22 APU after 5000 h at 740°C outside cathode contact.

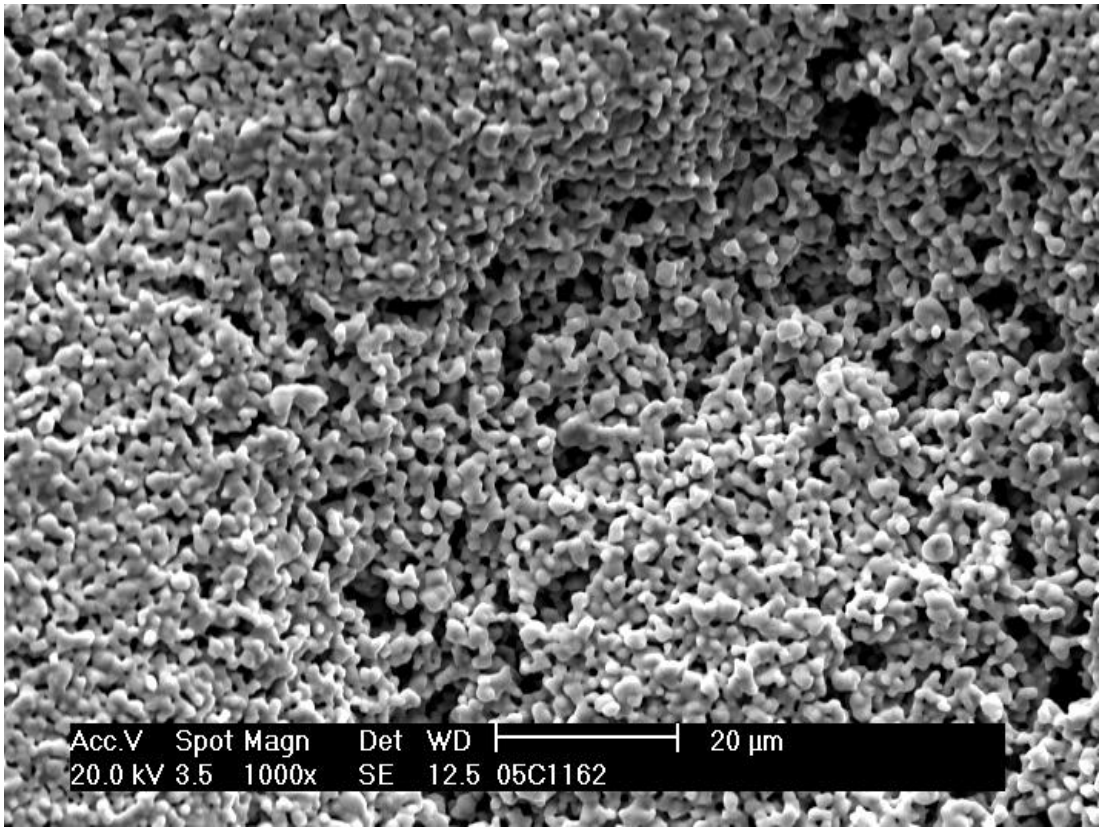

Fig. 53. The appearance of the cathode side cell surface after 500 h at 740°C in contact with Crofer 22 APU.

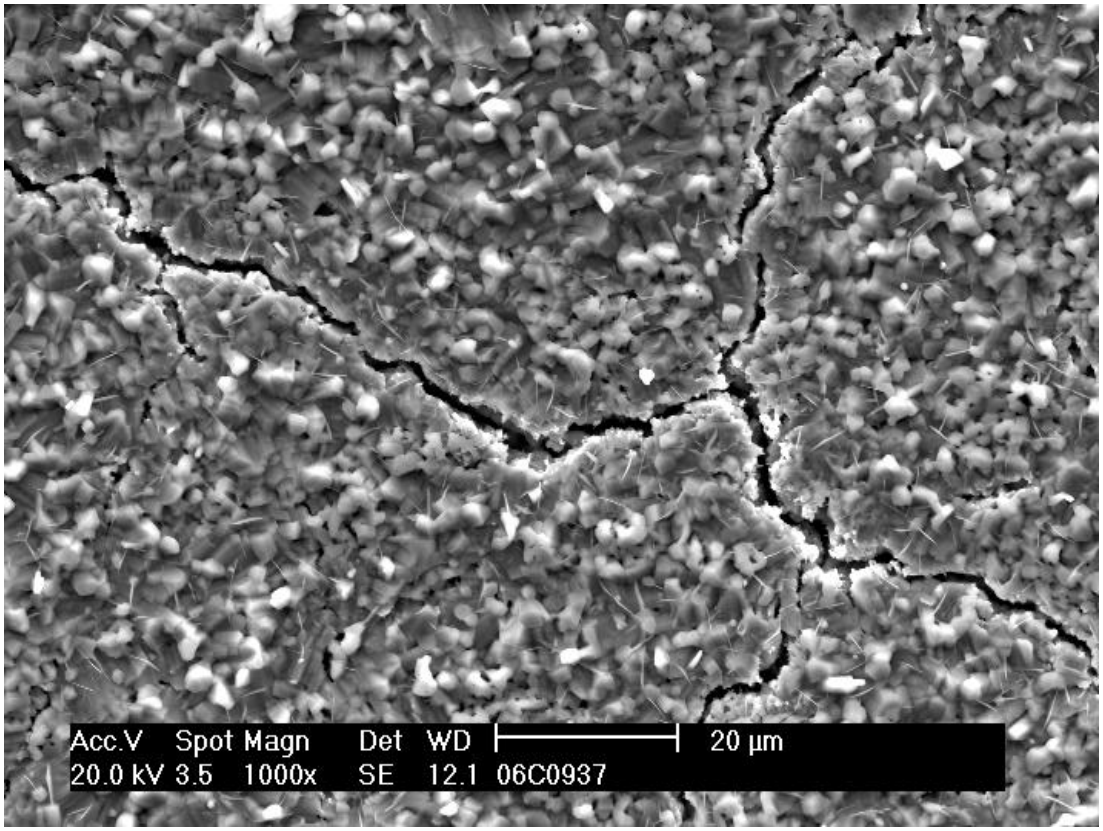

Fig. 54. The appearance of the cathode side cell surface after 5000 h at 740°C in contact with Crofer 22 APU.

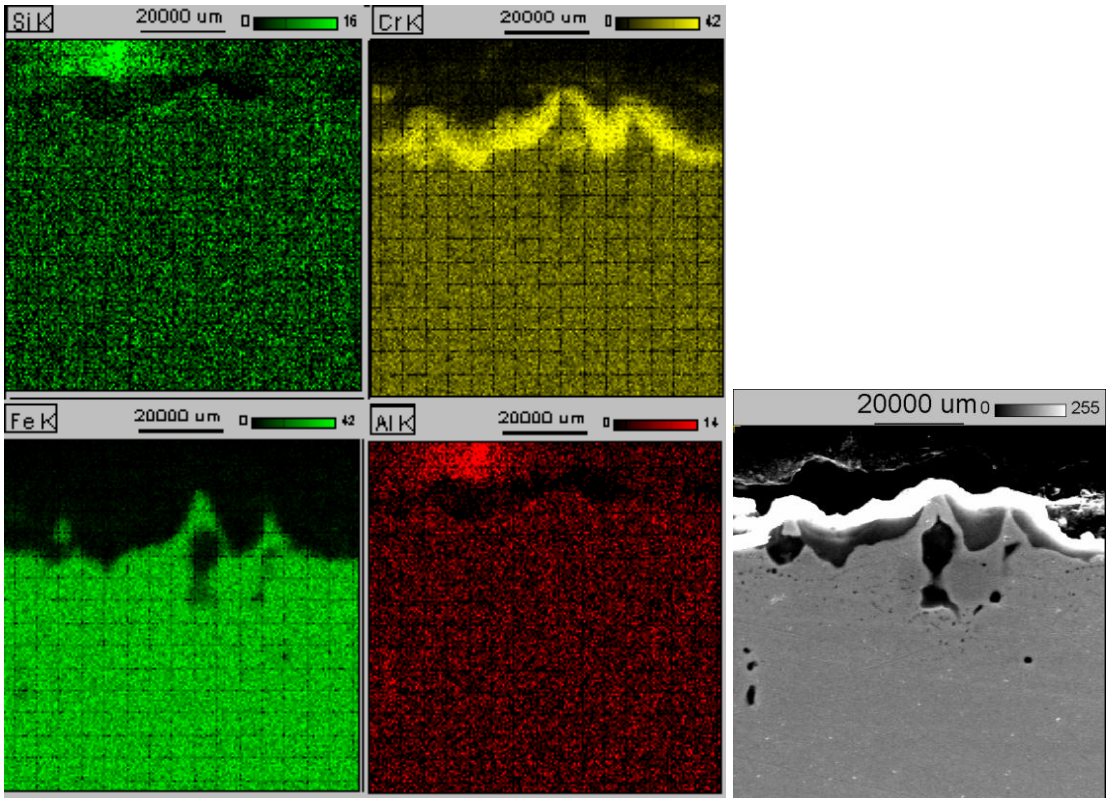

Fig. 55. Element maps of Si, Cr, Fe and Al for the Crofer 22 APU surface after 5000 h of exposure (outside cathode contact); actual scale 10µm.

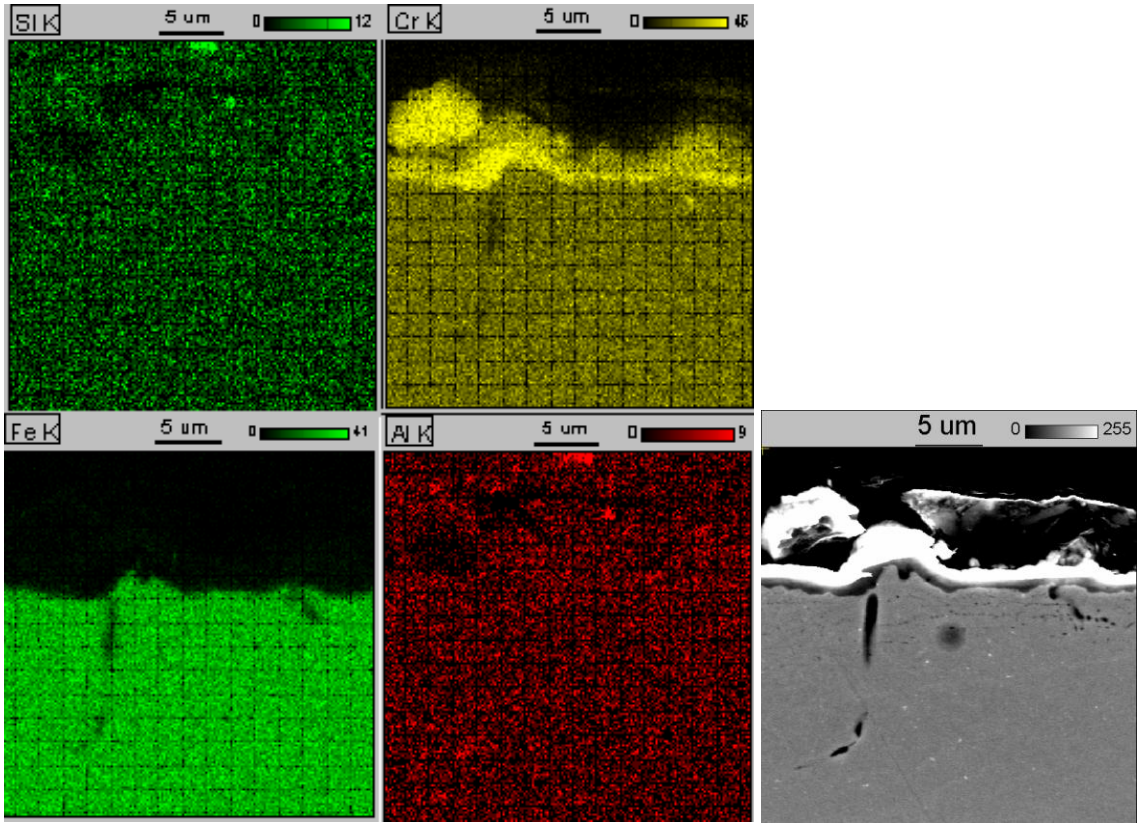

Fig. 56. Element maps of Si, Cr, Fe and Al for the Crofer 22 APU surface after 5000 h of exposure (cathode contact).

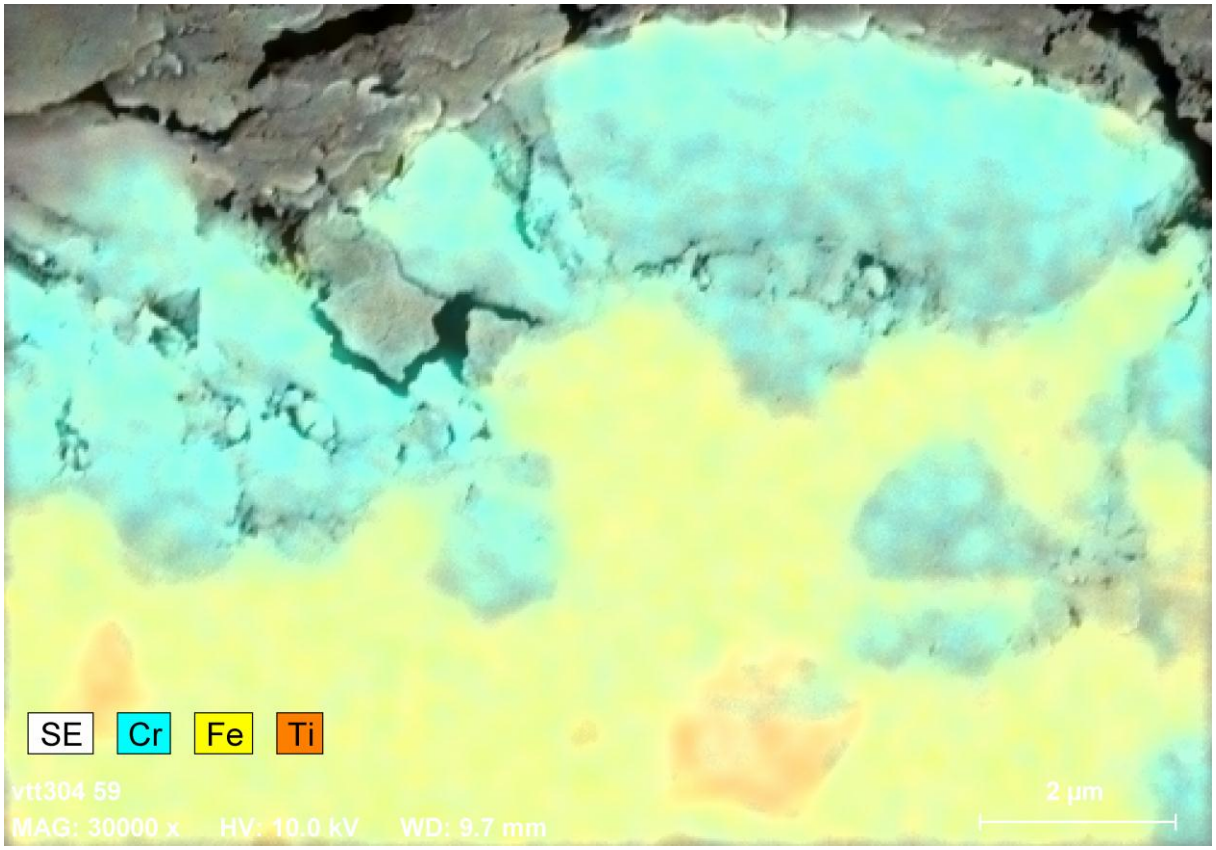

Fig. 57. Element map of Cr, Fe and Ti for Crofer 22 APU surface cross section after 5000 h of exposure (cathode contact).

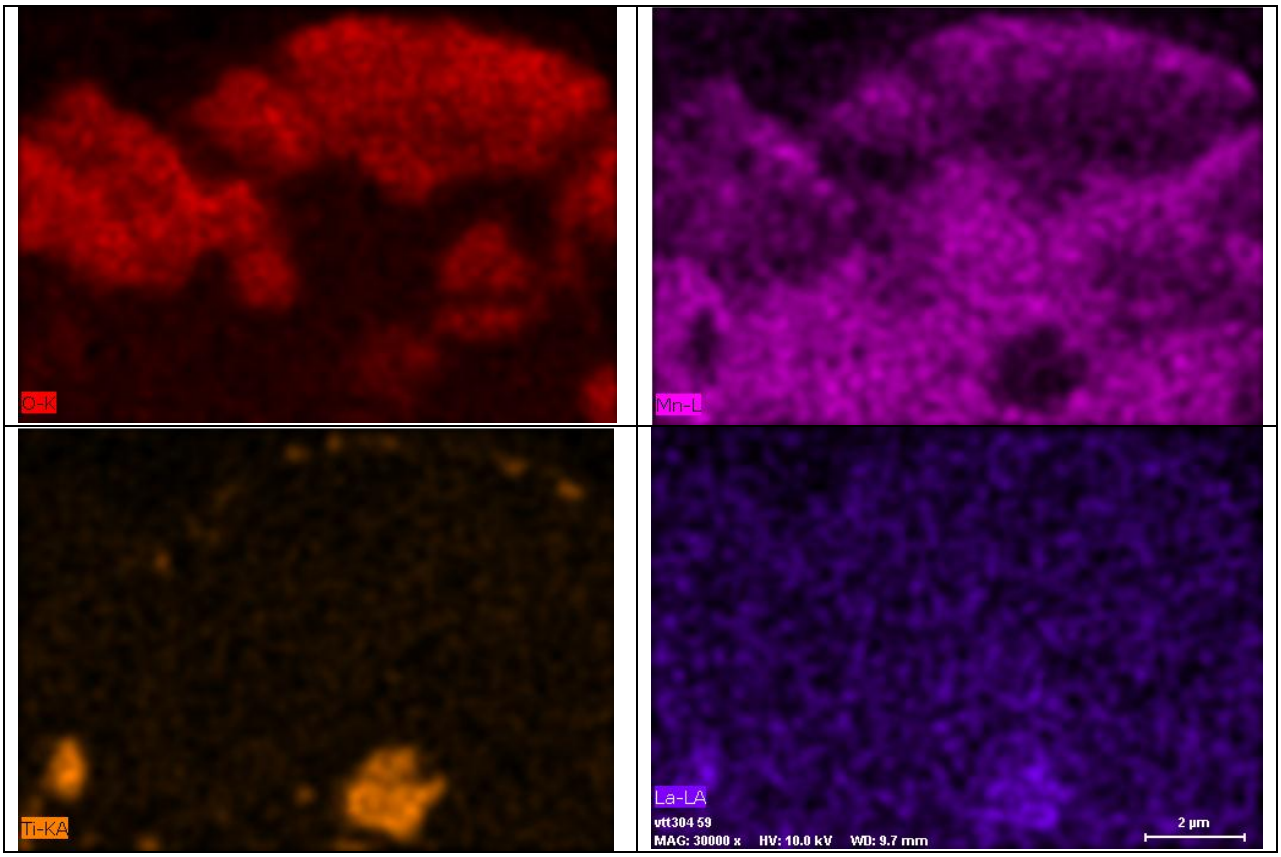

Fig. 58. Element maps of O, Mn, Ti and La for Crofer 22 APU surface cross section at the same location as in Fig. 57

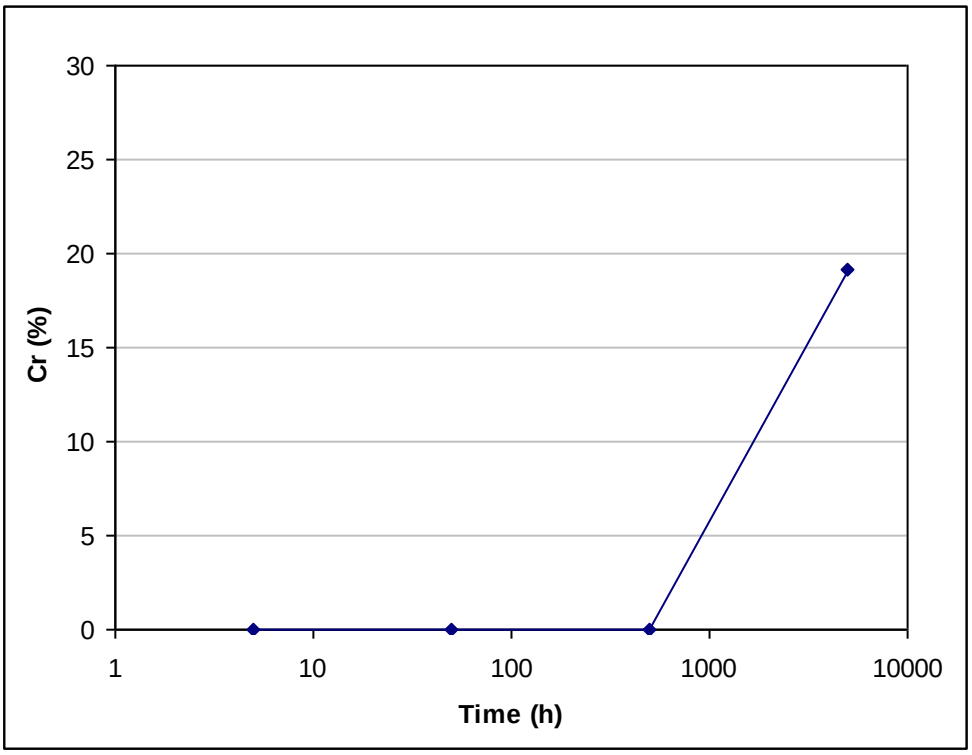

Fig. 59. The chromium content on the contact surface of the SOFC cell (with Crofer 22 APU, EDS analysis).

3.4.2 Microstructural evolution of Crofer 22 APU

The effect of exposure at 740°C on the microstructures of Crofer 22 APU is shown in Fig. 60 to Fig. 62 for the initial state and after 500 and 5000 h. It can be seen that at this level of detail, the main change of the microstructure is limited to grain growth. In comparison with alloy 430 and ZMG 232, the Crofer 22 APU test coupons showed less inclusions (carbides) in both as-new state and after 5000 h of exposure.

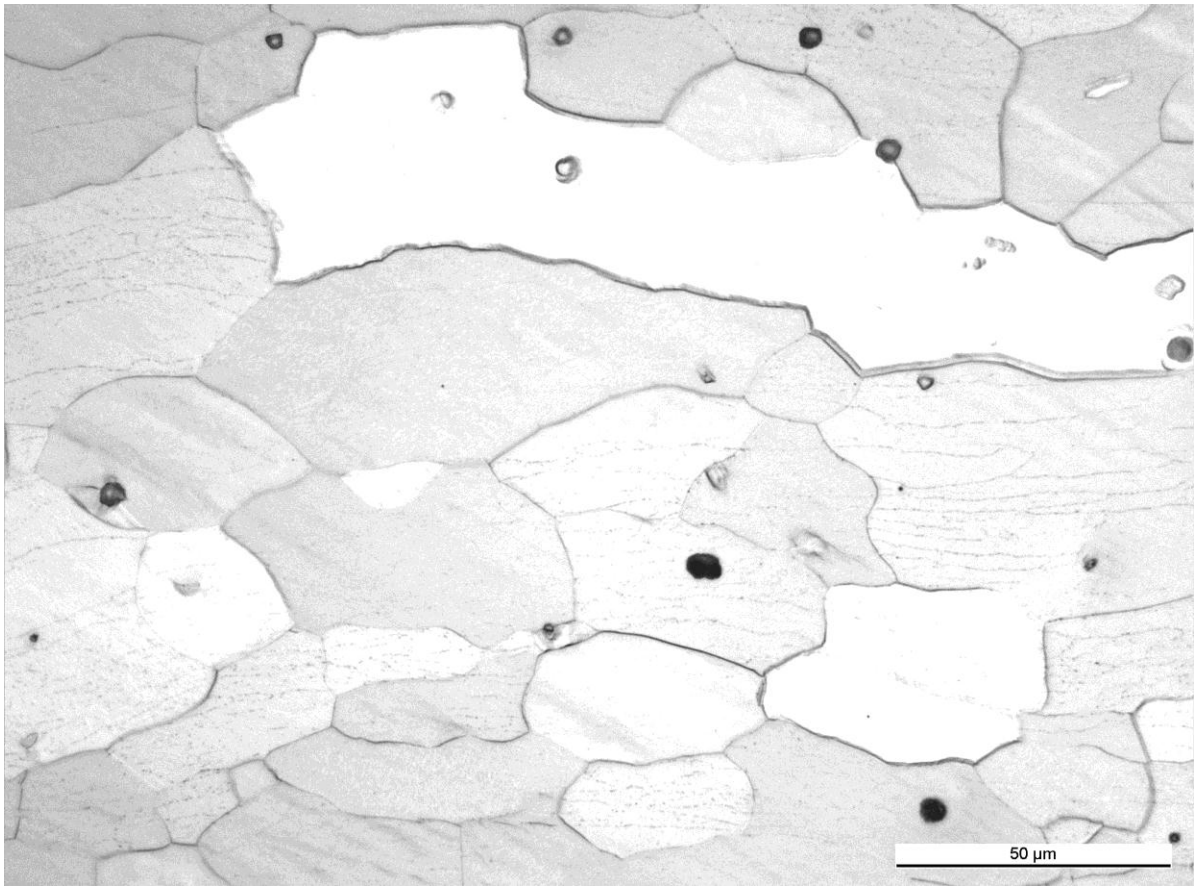

Fig. 60. The microstructure of Crofer 22 APU as received.

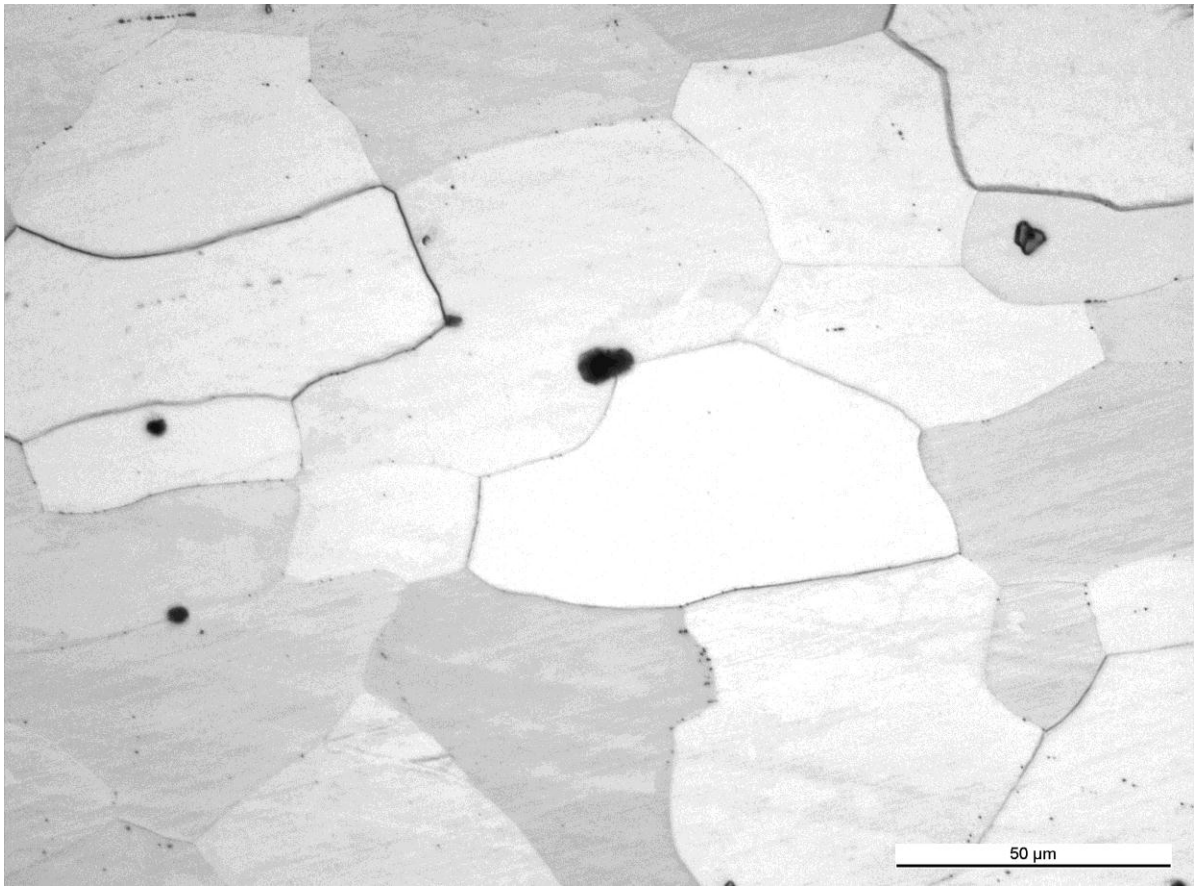

Fig. 61. The microstructure of Crofer 22 APU after 500 h of exposure.

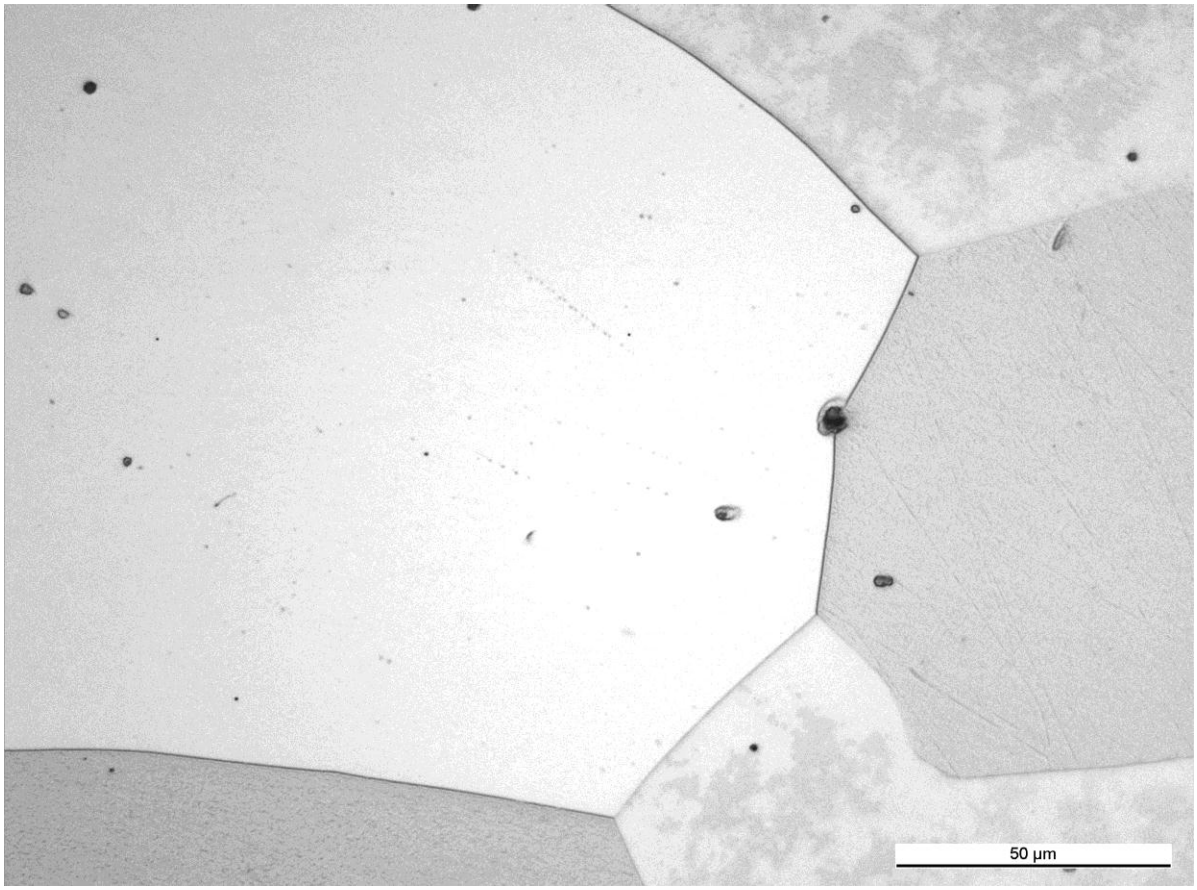

Fig. 62. The microstructure of Crofer 22 APU after 5000 h of exposure.

4 Discussion

In case of alloy 430, annealing at 740°C up to 5000 h resulted in some precipitation and coarsening of carbides at the grain boundaries but no significant grain growth (Fig. 20 to Fig. 22). No similar change in the grain boundary carbides was observed in ZMG 232 and Crofer 22 APU, but these alloys exhibited clear grain growth and some coarsening of intragranular precipitates during annealing.

The observed mass change of the test coupons shows reasonable agreement with parabolic oxidation at least up to 500 h (Fig. 3). This is also shown by the fitted expressions (1) to (3) where the exponent for time was 0.52 ± 0.10. Of the test materials, alloy 430 showed slowest and alloy ZMG 232 fastest oxidation rate up to 500 h. By 5000 h of testing, especially Crofer 22 APU and alloy 430 show signs of oxide spallation, indicated as downward deviation from the parabolic trend line (Fig. 3). The oxides that did not spall were about 3-4 µm in thickness after 5000 h at 740°C. Up to 5000 h of exposure, ZMG 232 showed no clear deviation from the parabolic trend line. It is notable that alloy 430 showed the lowest rate of mass change although it also has the lowest Cr content of the tested alloys. The results regarding mass change in dry laboratory air are compared with literature data on similar exposure at 700 – 900°C in Table 2 and in Fig. 63. It can be seen that the oxidation rate constants from the present study are higher than those taken from the literature. Some of the reasons could be related to much shorter testing times in the other studies [1-5]. However, the isothermal range of the k_p-values for the three materials (about one order of magnitude) appears to be

approximately similar in the present work and in the literature data. Also, the general order of the materials seems to be the same.

Table 2. Comparison of mass change at 700 to 900°C from [1-5] and this work (*).

Material	Cyclic/static	Temperature (°C)	Specimen thickness (mm)	$k_p = x^2/t$ [mg^2/(cm^{4}h)]	Total exposure time (h)	Source
Crofer 22 APU	static	740	2.5/3.0	$5.4 \cdot 10^{-3}$	500	*
	static	800	2.5	$1.73 \cdot 10^{-3}$	100	[1]
	static 1)	800	0.5	$2.88 \cdot 10^{-3}$ $1.01 \cdot 10^{-3}$	1000	[4]
	cyclic 2)	800	2	$2.34 \cdot 10^{-3}$	1000	[2]
	cyclic 2)	900	2	$3.60 \cdot 10^{-2}$	1000	[2]
ZMG 232	static	740	2.5/3.0	$14.5 \cdot 10^{-3}$	500	*
	cyclic 2)	800	1	$9.72 \cdot 10^{-3}$	1000	[2]
Alloy 430	static	740	2.5/3.0	$2.4 \cdot 10^{-3}$	500	*
	static	800	1-1.3	$3.06 \cdot 10^{-3}$	100	[3]
	static	700	1	$1.44 \cdot 10^{-5}$	100	[5]
	static	750	1	$9.41 \cdot 10^{-5}$	100	[5]
	static	800	1	$2.89 \cdot 10^{-4}$	100	[5]

1) *two batches tested*
2) *cyclic; 2h heating /15 min cooling*

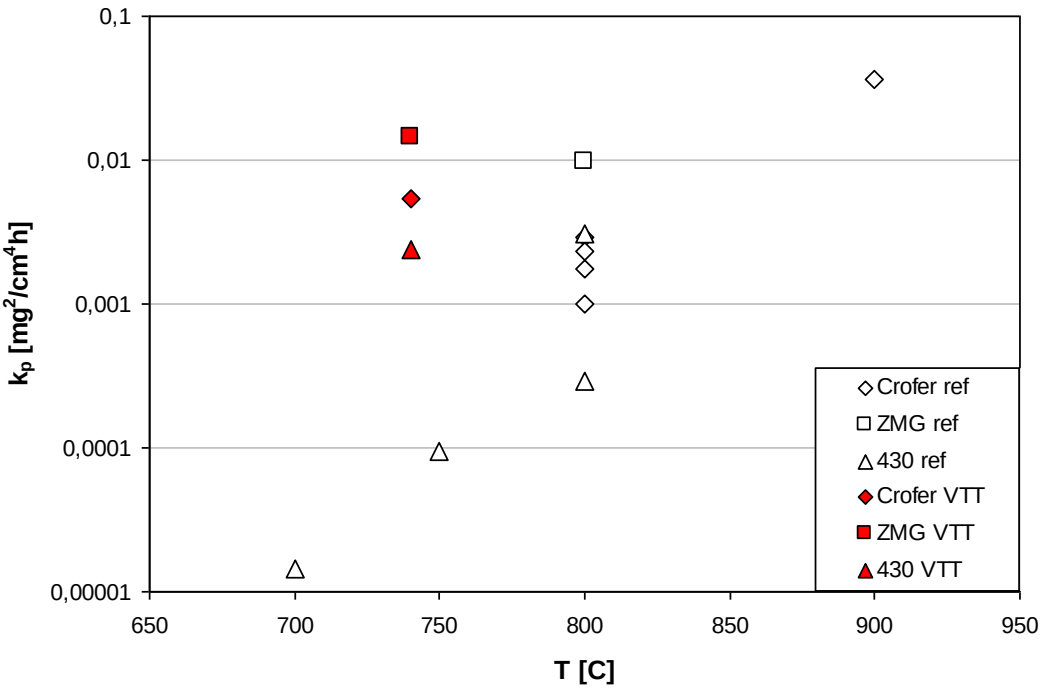

Fig. 63. The oxidation rate constants of the tested alloys from Table 2.

During oxidation up to 5000 h, the observed changes in the chemical composition of the surfaces were mostly similar for all tested alloys (Fig. 4, Fig. 23 and Fig. 44). The Fe content of the oxidised surface decreased to 3-13% in this time, while the Mn content increased to about 22-30%. The surface Cr content was about 35-40% after 500 h, and thereafter remained constant or decreased somewhat to about 25-40%. The observed small long term decrease in the surface Cr content could be due to surface evaporation at the annealing temperature. No significant difference was observed in the surface composition of any of the three alloys when comparing the regions within and outside the contact to the cell.

The oxide surface of alloy 430 was relatively uniform after annealing up to 5000 h. The cross section shows a dense oxide layer with essentially no additional precipitates under the oxide (Fig. 10). Cr content of the oxide appears highest near the top surface while Si content is highest next to the metal (Fig. 13 and Fig. 14). The oxide surfaces on ZMG 232 and Crofer 22 APU show distinct differences between the grain boundaries and grain interiors of the oxide. Apparently Cr- and Mn-rich oxides are precipitating at the boundaries to give an appearance of a nearly continuous network (Fig. 24 and Fig. 45). The boundary oxide precipitates appear to further coarsen during annealing, particularly clearly in Crofer 22 APU (Fig. 46). In the surface cross sections again a nearly continuous Cr-rich oxide appears on top and a Si-rich discontinuous layer next to the metal. In addition, below the oxide there is a layer containing relatively large Al- and Ti-rich precipitates, which are apparently only partly oxides (Fig. 29 and Fig. 50). For all tested alloys in contact with the cell cathode, the Cr content on the cell surface started to increase by 500 to 5000 h of annealing (Fig. 64). Hence Cr evaporation is likely to be an issue for all alloys in long term service at about 740°C. Cr evaporation from these alloys is probably significant even at lower temperatures, as suggested by parallel experience from Cr containing alloys in other applications of power and process engineering. This further suggests that even steels like ZMG 232 and Crofer 22 APU that have been designed for SOFC interconnectors would require protective coatings to avoid Cr poisoning of the cathode.

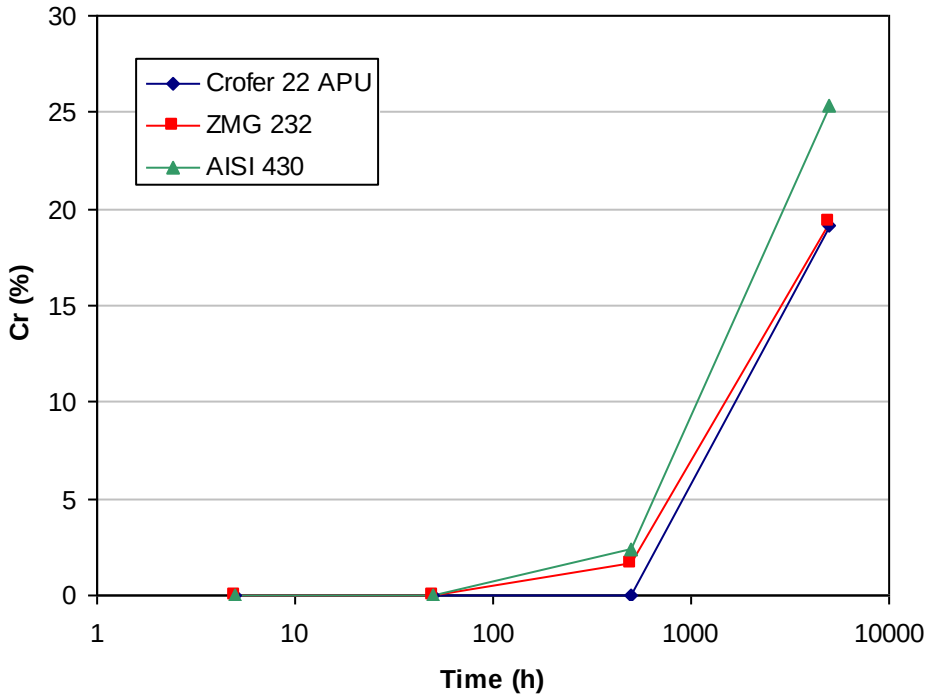

Fig. 64. The chromium content on the contact surface of the SOFC cell (with tested bipolar plate alloys, EDS analysis).

5 Summary

Oxidation and degradation behaviour has been studied for three ferritic stainless steels as candidate SOFC interconnector alloys. Regarding internal thermal change, exposure at 740°C up to 5000 h mainly resulted in grain boundary carbide coarsening in alloy 430, and mainly in grain growth in alloys ZMG 232 and Crofer 22 APU. Of the tested materials, alloy 430 showed slowest and ZMG 232 highest oxidation rate in dry air. The mass change was reasonably consistent with parabolic oxidation at least up to 500 h, while by 5000 h of exposure Crofer 22 APU and alloy 430 (but not ZMG 232) showed signs of oxide spallation. Alloy 430 showed the lowest initial oxidation rate, although it also has the lowest Cr content. The oxides that did not spall were about 3-4 µm in thickness after 5000 h at 740°C. In general, the oxidation rate constants from this work are higher than those taken from the literature, but in a similar isothermal range and in the same materials order.

Up to 5000 h the chemical composition of the surface oxide showed mostly similar change for all tested alloys, with decreasing Fe content from 65-75% to 2-12% and increasing Mn content from near zero to 22-30%. The Cr content of the oxide increased from 18-22% to 35-41% in 500 h and was thereafter constant or slightly decreasing to about 24-40% after 5000 h. No significant difference was observed in the surface composition of any of the three alloys when comparing the regions within and outside the contact to a cell cathode surface. The oxide surface of alloy 430 was relatively uniform and there were no distinct precipitates below the top oxide. The oxide surfaces on ZMG 232 and Crofer 22 APU showed Cr- and Mn-rich oxides precipitating at the oxide grain boundaries to form a nearly continuous network that was further coarsening during annealing. All alloys showed a nearly continuous Cr-rich layer on top, and a Si-rich discontinuous layer next to the metal. Below the surface oxides the alloys ZMG 232 and Crofer 22 APU showed a layer with relatively large Al- and Ti-rich precipitates.

For all tested alloys in contact with the cell cathode, the Cr content of the cell surface started to increase by 500 to 5000 h of exposure. Therefore, Cr evaporation is likely to be an issue for all alloys in long term service at comparable temperature levels, and probably even at lower temperatures. Protective solutions to avoid Cr poisoning of the cathode would be necessary even for steels like ZMG 232 and Crofer 22 APU that have been designed for SOFC interconnector service.

References

1. Piccardo P. et al. Metallic interconnect for SOFC: Characterization of their corrosion resistance in hydrogen/water atmosphere and at the operating temperatures of differently coated metallic alloys. Surface & Coating Technology 201, 2006, p. 4471-4475.
2. Huczkowski P. et al. Oxidation limited life times of chromia forming ferritic steels. Materials and Corrosion, Volume 55, No. 11, 2004, p. 825-830.
3. Brylewski T. et al. Application of Fe-16Cr ferritic alloy to interconnector for a solid oxide fuel cell. Solid State Ionics. Volume 143, Issue 2, June 2001, p.131-150
4. Antepara I. et al. Evaluation of ferritic steels for use as interconnects and porous metal supports in IT-SOFCs. Journal of Power Sources 151, 2005, p. 103-107.
5. Qu W., Jian L., Douglas G., Hill J. Yttrium, cobalt and yttrium/cobalt oxide coatings on ferritic stainless steels for SOFC interconnects. Journal of Power Sources 157 (2006) 335-350, doi: 10.1016/j.jpowsour.2005.07.052